



## The curious and intricate case of the European *Hediste diversicolor* (Annelida, Nereididae) species complex, with description of two new species

Marcos A. L. Teixeira, Torkild Bakken, Pedro E. Vieira, Joachim Langeneck, Bruno R. Sampieri, Panagiotis Kasapidis, AscensãO Ravara, Arne Nygren & Filipe O. Costa

To cite this article: Marcos A. L. Teixeira, Torkild Bakken, Pedro E. Vieira, Joachim Langeneck, Bruno R. Sampieri, Panagiotis Kasapidis, AscensãO Ravara, Arne Nygren & Filipe O. Costa (2022) The curious and intricate case of the European *Hediste diversicolor* (Annelida, Nereididae) species complex, with description of two new species, Systematics and Biodiversity, 20:1, 1-39, DOI: [10.1080/14772000.2022.2116124](https://doi.org/10.1080/14772000.2022.2116124)

To link to this article: <https://doi.org/10.1080/14772000.2022.2116124>

 View supplementary material 

 Published online: 17 Oct 2022.

 Submit your article to this journal 

 Article views: 398

 View related articles 

 View Crossmark data 

## Research Article



# The curious and intricate case of the European *Hediste diversicolor* (Annelida, Nereididae) species complex, with description of two new species

MARCOS A. L. TEIXEIRA<sup>1,2</sup> , TORKILD BAKKEN<sup>3</sup> , PEDRO E. VIEIRA<sup>1,2</sup> ,  
JOACHIM LANGENECK<sup>4</sup> , BRUNO R. SAMPIERI<sup>5</sup> , PANAGIOTIS KASAPIDIS<sup>6</sup> ,  
ASCENSÃO RAVARA<sup>7</sup> , ARNE NYGREN<sup>8</sup>  & FILIPE O. COSTA<sup>1,2</sup> 

<sup>1</sup>Centre of Molecular and Environmental Biology (CBMA), Department of Biology, University of Minho, Campus de Gualtar, Braga, 4710-057, Portugal

<sup>2</sup>Institute of Science and Innovation for Bio-Sustainability (IB-S), University of Minho, Campus de Gualtar, Braga, 4710-057, Portugal

<sup>3</sup>Norwegian University of Science and Technology, NTNU University Museum, Trondheim, NO-7491, Norway

<sup>4</sup>Dipartimento di Biologia, Università di Pisa, via Derna 1, Pisa, I-56126, Italy

<sup>5</sup>Museu de Zoologia, Instituto de Biologia, Universidade Estadual de Campinas – IB/UNICAMP, Rua Charles Darwin, Bloco N, Cidade Universitária, Campinas, SP, Brasil

<sup>6</sup>Hellenic Centre for Marine Research, Institute of Marine Biology, Biotechnology and Aquaculture, Anávyssos, Greece

<sup>7</sup>Centre for Environmental and Marine Studies (CESAM), Department of Biology, University of Aveiro, Campus de Santiago, Aveiro, 3810-193, Portugal

<sup>8</sup>Institutionen for marina vetenskap, Göteborgs Universitet, Tjärnö, Strömstad, Sweden

(Received 23 February 2022; accepted 18 August 2022)

Past molecular studies using mtDNA sequences and alloenzymes signalled the existence of at least two cryptic species within the *Hediste diversicolor* morphotype, in European coasts. However, to this day, no new species descriptions have been made. In this study, we identified five completely sorted lineages using a multi-locus approach, including the mitochondrial DNA cytochrome oxidase I gene (COI-5P) and the nuclear markers ITS2 rRNA and 28S rRNA. The molecular data were complemented with morphometric measurements examined through multivariate statistical analysis and the incorporation of statistical dissimilarities. Apart from the Baltic Sea, where three of the lineages occur in sympatry, *Hediste diversicolor* comprises four deeply divergent allopatric lineages in the rest of Europe. They group populations from the NE Atlantic and part of the Western Mediterranean Sea; from the Tyrrhenian Sea; from the Adriatic and Ionian Sea; and, lastly, from the Caspian, Black and the northern Aegean Seas. The lineage from the Ionian Sea revealed low genetic distances compared with the one from the Adriatic Sea and lacked enough specimens for the morphometric analysis, preventing further conclusions about its independent status. Three independent morphometric clusters were identified mainly based on worm size, the distance between the anterior and posterior eyes, parapodia proportions and the length of several prostomial appendages. Two sympatric lineages present in the Baltic Sea, showed evidence of possible hybridization and lacked significant PCA morphometric variation between them. The two remaining lineages were formally described as new species, namely *Hediste pontii* sp. nov. (Adriatic Sea) and *Hediste astae* sp. nov. (northern Aegean, Caspian and Black Seas). These new species can now be formally recognized and used in biomonitoring or other relevant ecological studies. Finally, a neotype is defined for *H. diversicolor*, whose usage is restricted to the NE Atlantic lineage.

<http://www.zoobank.org/urn:lsid:zoobank.org:pub:948C73FC-B07F-40A3-B8FA-03B60DE2089D>

**Key words:** Annelida, cryptic species, *Hediste*, mitochondrial DNA, morphometry, nuclear DNA

## Introduction

The common ragworm *Hediste diversicolor* (O. F. Müller, 1776) (Nereididae) is a widespread omnivorous

species which occurs in estuarine environments and brackish waters among mud, sand, gravel and turf of the Atlantic coasts of Europe, and in the Mediterranean, Black and Caspian Seas (Scaps, 2002). It is suspected that this species was also introduced to North America prior to 1880, hence earlier than the first biological

Correspondence to: Marcos A. L. Teixeira. E-mail: [mark-us\\_teixeira@hotmail.com](mailto:mark-us_teixeira@hotmail.com)

surveys of the intertidal sediment in the NW Atlantic (Einfeldt *et al.*, 2014), where the most probable vector was the dry ballast, i.e. stored sediment or soil from the intertidal onto ships to adjust buoyancy (Galil *et al.*, 2011). This seems to be corroborated by the occurrence of this species in estuarine sediment associated with historic shipping ports and the brooding of larvae lacking a pelagic phase (Faulwetter *et al.*, 2014; Scaps, 2002). This species lacks a true planktonic larval phase in early development and its life cycle is completed within the low-salinity regions of estuaries, without epitokous metamorphosis and reproductive swarming in adults (Smith, 1950). The larvae burrow immediately after emergence, resulting in limited dispersal that is expected to promote genetic isolation among populations separated by stretches of unsuitable habitat at different spatial ranges (Bartels-Hardege & Zeeck, 1990; Scaps, 2002). *Hediste diversicolor* is an efficient bioturbator that builds U- or Y-shaped burrows at densities documented to exceed 3500 individuals  $m^{-2}$  and has an important role in the biogeochemical and ecological processes of estuarine environments, as well as representing an important prey for many invertebrate and vertebrate species (Bowser *et al.*, 2013; Cuny *et al.*, 2007). This species is also one of the few nereidids of economic importance, used as bait in recreational fishing and as food in aquaculture (Scaps, 2002; Younsi *et al.*, 2010). It is commonly used in ecotoxicological studies, bioaccumulation assays (Burlinson & Lawrence, 2007; Durou *et al.*, 2007; Virgilio *et al.*, 2005) and displays a wide tolerance to temperature changes (Wolff, 1973), hypoxia (Kristensen, 1983) and salinity variation, thriving in habitats ranging from fresh water to twice the normal salinity found in seawater (Neuhoff, 1979; Wolff, 1973). However, it is susceptible to anthropogenic stress, experiencing reduced fecundity and fitness when exposed to elevated levels of toxic trace metals (Durou *et al.*, 2005; Moreira *et al.*, 2006; Scaps, 2002). Yet, it still possesses higher tolerance to heavy metals compared with other nereidid species (Hateley *et al.*, 1992), making it a resilient bio-indicator in many marine and brackish water habitats.

Past studies have suggested inter-population morphological, biochemical and physiological differences within this species in individuals from different areas and different environmental conditions, which may be related to the limited dispersal capacity of the species (Scaps, 2002). For example, differences in the number of paragnaths were reported by Maltagliati *et al.* (2006) but no geographic pattern of morphological variation was detected by multidimensional scaling. This suggests that the variation found among populations may reflect local differences in diet or dominant mode of feeding, and

thus be the consequence of phenotypic plasticity (Forsman, 2015; Fusco & Minelli, 2010). Genetic data also hinted at the existence of at least two cryptic species. Using both mitochondrial and nuclear markers, Audzijonyte *et al.* (2008) divided *Hediste diversicolor* into Species A and B, both sympatric in the Baltic Sea. Later, Virgilio *et al.* (2009) found haplotypes of species B in the western Mediterranean, Adriatic Sea, as well as in the Black and Caspian Seas, with three deeply divergent mitochondrial DNA lineages with a nearly disjunct geographic distribution and suggested species B was introduced from these areas to the Baltic in two or more colonization events. Species A was also reported in North America from the Bay of Fundy and Maine, with the Maine population having unique haplotypes and most likely originated from unsampled European populations (Einfeldt *et al.*, 2014). More recently, Vasileiadou *et al.* (2016) analysed populations in the Greek Amvrakikos Gulf and found unique COI haplotypes which are distinct from the ones reported in the previous studies.

The aim of this study was to employ a multi-locus approach together with morphometric analysis to complement the existing evidence of separate species within the European *Hediste diversicolor* populations. Naming of newly found cryptic species is fundamental for their subsequent routine recognition and to achieve realistic estimates of biodiversity (Delić *et al.*, 2017; Fišer *et al.*, 2018; Hutchings & Kupriyanova, 2018). Failure to do so prevents their use in large-scale biomonitoring programmes, even those employing DNA-based approaches, and limits our understanding of their evolutionary and ecological significance, generating biased interpretations in ecotoxicological, bioaccumulation and in other relevant ecological studies (Hutchings & Kupriyanova, 2018; Volkenborn *et al.*, 2007).

## Materials and methods

### Taxon sampling and molecular data retrieval

We gathered a total of 269 *Hediste* specimens distributed along the European coasts (Table 1) by digging out 10–20 cm thick of sediment and washing it through a 1-mm sieve in low tide or near the shore at 0.5–1 m depth. From Portugal, samples were collected in the estuaries of Sado, Lima and Minho, as well in the Aveiro lagoon. From Spain, specimens were collected in Vigo (Lagares Estuary) and Coruña (Ferrol Lagoon). Specimens were also collected in the north of France (Brest), south Norway (Grimstad and Sandefjord), middle Norway (Trondheim), Sweden (Tjärnö-Saltö canal) and Italy,

**Table 1.** Number of specimens acquired for this study, the respective sampling area, coordinates and code abbreviation for the different sampling locations and the institution responsible for storing the vouchers.

Code	Region	Location	n	Coordinates		Institution storing
				Latitude	Longitude	
SA	NE European Coast	Portugal, Sado Estuary	18	38°29'52.8"N	8°50'16.8"W	DBUA
			9	38°29'24.0"N	8°48'54.0"W	
AV	NE European Coast	Portugal, Aveiro Lagoon	25	40°38'02.4"N	8°40'30.0"W	
LI	NE European Coast	Portugal, Lima Estuary	23	41°42'03.6"N	8°44'56.4"W	
MI	NE European Coast	Portugal, Minho Estuary	25	41°52'55.2"N	8°49'44.4"W	
LA	NE European Coast	Spain, Lagares Estuary	5	42°12'07.2"N	8°46'40.8"W	
FE	NE European Coast	Spain, Ferrol Lagoon	10	43°29'34.8"N	8°14'56.4"W	
BR	NE European Coast (Celtic Sea)	France, Brest	10	48°24'21.6"N	4°22'01.2"W	
TD	North European Sea	Norway, Trondheim	2	63°26'09.6"N	10°29'56.4"E	NTNU
GM	Skagerrak	Norway, Grimstad	5	58°17'52.8"N	8°32'20.4"E	
SF	Skagerrak	Norway, Sandefjord	1	59°07'37.2"N	10°14'24.0"E	
TJ	Kattegat Sea	Sweden, Tjörnö-Saltö canal	52	58°52'26.4"N	11°08'42.0"E	DBUA
NA	Tyrrhenian Sea (Mediterranean)	Italy, Navicelli Canal	10	43°40'19.2"N	10°22'15.6"E	
VE	Adriatic Sea (Mediterranean)	Italy, Venezia Lagoon	28	45°20'13.2"N	12°16'30.0"E	
AM	Ionian Sea (Mediterranean)	Greece, Amvrakikos Lagoon	5	39°02'45.6"N	20°46'15.6"E	DNA only
NAS	Northern Aegean Sea (Mediterranean)	Greece, Evros Lagoon	30	40°44'38.4"N	26°02'13.2"E	DBUA
		Greece, Ptelea Lagoon	8	40°56'13.2"N	25°14'49.2"E	
		Greece, Aliki Lagoon	6	40°57'00.0"N	25°12'50.4"E	
		Greece, Nestos Lagoon	4	40°54'36.0"N	24°52'22.8"E	
		Greece, Axios Lagoon	4	40°30'28.8"N	22°43'40.8"E	

from both the western Mediterranean (Navicelli Canal, Pisa) and eastern Mediterranean Sea (Venezia Lagoon). Lastly, additional specimens were obtained from the Ionian Sea in the Amvrakikos Lagoon (Greece), as well in eastern Greece from lagoons in the Thracian Sea, or most commonly known as northern Aegean Sea (Evros, Nestos, Alyki, Axios and Ptelea). Twenty-five specimens from Evros Lagoon (DBUA0002466.07.v01-v13 and DBUA0002466.08.v01-v12) were preserved in formaldehyde and the remaining ones were all preserved in 96% ethanol.

We sequenced 211 *Hediste* specimens for the mitochondrial cytochrome oxidase subunit I (mtCOI-5P). A representative number of specimens per location for the ITS2 region and 28S rRNA were used (with 93 nuclear sequences in total). Molecular data from 12 specimens of *Alitta virens* (Sars, 1835), a nereidid species commonly found living among individuals of *H. diversicolor* and morphologically close to the latter species when analysing small specimens, were used as outgroup for all the analysed loci (12 COI and 3 ITS2/28S sequences). “Species A” and “Species B” were defined after Audzijonyte et al. (2008), and representative sequences from the Baltic Sea corresponding to each of the obtained MOTUs were used for comparison purposes. Additionally, COI GenBank sequences of ‘Species B’ (Virgilio et al., 2009) from the western Mediterranean, Adriatic Sea and Black and Caspian Seas, together with sequences of ‘Species A’ from Great Britain, Germany and the Netherlands were added to the alignment. Lastly, COI sequences from Vasileiadou et al. (2016)

corresponding to the new Mediterranean haplotypes and two COI sequences from Massachusetts, USA (PBCB Bioblitz 2016 BOLD project) were added as well to comprise the final dataset. DNA was extracted, amplified, sequenced, and assembled as described in Lobo et al. (2016). For the PCR conditions and primers see Supplemental Table S1.

The dataset used for molecular analysis and its meta-data can be accessed at BOLD under the project ‘*Hediste* species complex (DS-MTHD)’, in the following DOI link: [dx.doi.org/10.5883/DS-MTHD](https://dx.doi.org/10.5883/DS-MTHD). GenBank accession numbers for the original data are: OP038674-OP038788, OP038790-OP038834, OP038836-OP038897 (COI); OP028540-OP028635 (ITS2) and OP028725-OP028820 (28S). The biological material is deposited at the Research Collection of Marine Invertebrates of the Department of Biology of the University of Aveiro (CoBI-DBUA), Portugal. Specimens from Norway are deposited at the Norwegian University of Science and Technology, NTNU University Museum (Bakken et al., 2021). Specimens which were exhausted in the DNA analysis were assigned only with the Process ID from BOLD (<http://v4.boldsystems.org/>), corresponding to the ones from the Amvrakikos Lagoon (MTHD178-20, MTHD180-20, MTHD183-20, MTHD184-20 and MTHD187-20), Ferrol Lagoon (MTHD015-20) and Tjörnö-Saltö Canal (MTHD145-20). Sampling locations, GenBank accession numbers per specimen, and voucher data for both the original data and former studies used for comparison purposes are detailed in Supplemental Table S2.

## Phylogenetic analysis

The phylogenetic analyses were performed through maximum likelihood (ML) and Bayesian inference (BI). Mitochondrial COI sequences and the nuclear markers (ITS2 and 28S) were aligned separately with MAFFT online (<https://mafft.cbrc.jp/alignment/server/>; Katoh & Standley, 2013) and concatenated with MEGA 10.0.05 (Kumar *et al.*, 2018). The sequence lengths for the different markers are included in [Supplemental Table S1](#). Highly variable regions, extensive gaps and poorly aligned positions in the concatenated alignment were eliminated using Gblocks 0.91 b ([http://molevol.cmima.csic.es/castresana/Gblocks\\_server.html](http://molevol.cmima.csic.es/castresana/Gblocks_server.html); Castresana, 2000), allowing all the options for a less stringent selection and not allowing many contiguous non-conserved positions, so that it becomes more suitable for phylogenetic analysis. We used MrBayes 3.1.2 (Ronquist & Huelsenbeck, 2003) to conduct the Bayesian analysis. Best-fit models were selected using the Akaike Information Criterion in the JModeltest software (Darriba *et al.*, 2012; Guindon & Gascuel, 2003). For COI we applied the Kimura-2-parameter model with gamma distributed rates across sites (K2P+G) for the first two positions and Hasegawa–Kishino–Yano (HKY) with equal rates across sites for the third position. The latter was also applied to the ITS2 and 28S loci. Number of generations was set to 10,000,000, and sample frequency to 500. Twenty-five per cent of the samples were discarded as burn-in (burninfrac = 0.25). The resulting tree file was checked for convergence in the effective sampling sizes (ESSs >200) with Tracer 1.6 software (Rambaut *et al.*, 2018) and then analysed in Figtree 1.4.3 (<http://tree.bio.ed.ac.uk/software/figtree/>). The final version of the concatenated tree was edited with the software Inkscape 0.92.3 (<https://www.inkscape.org>). Maximum likelihood phylogenies were performed in MEGA 10.0.05 with 1000 bootstrap runs with the HKY with equal rates across sites for the concatenated dataset. The BI tree was displayed in the results with the addition of the ML support values if a similar topology is found.

The alignments (fasta and nexus format) for each individual marker and the concatenated one are all publicly available online at Figshare (DOI: [dx.doi.org/10.6084/m9.figshare.19224600](https://doi.org/10.6084/m9.figshare.19224600)).

## MOTU clustering

To depict Molecular Operational Taxonomic Units (MOTUs), we applied three delineation methods to the concatenated alignment, except for COI where we also applied the Barcode Index Number (BIN), which makes use of the Refined Single Linkage (RESL) algorithm

implemented in BOLD (Ratnasingham & Hebert, 2013), exclusive to this locus. The Automatic Barcode Gap Discovery (ABGD; Puillandre *et al.*, 2012) was implemented on a web interface (<http://www.wabi.snv.jussieu.fr/public/abgd/abgdweb.html>) with default settings using the K2P distance matrix. The Generalized Mixed Yule Coalescent (GMYC) single threshold model (Fujisawa & Barraclough, 2013), as well the Poisson Tree Processes (bPTP; Zhang *et al.*, 2013) were applied, with both analyses performed on a web interface (<https://species.h-its.org/>). BEAST 2.4.6 (Bouckaert *et al.*, 2014) was used to generate the Bayesian ultrametric tree for the GMYC with the appropriate best model (based on AIC criteria; HKY equal rates), and four independent runs for 50,000,000 MCMC generations, sampled every 5000 generations. Tracer 1.6 software was used to estimate convergence ESSs > 200 for all parameters. The consensus tree was obtained using TreeAnnotator 2.4.6 (Bouckaert *et al.*, 2014) and loaded into the Figtree software. ML phylogenies obtained above in the ‘phylogenetic analysis’ section were employed for the bPTP results. A final consensus on MOTUs was chosen using the majority rule.

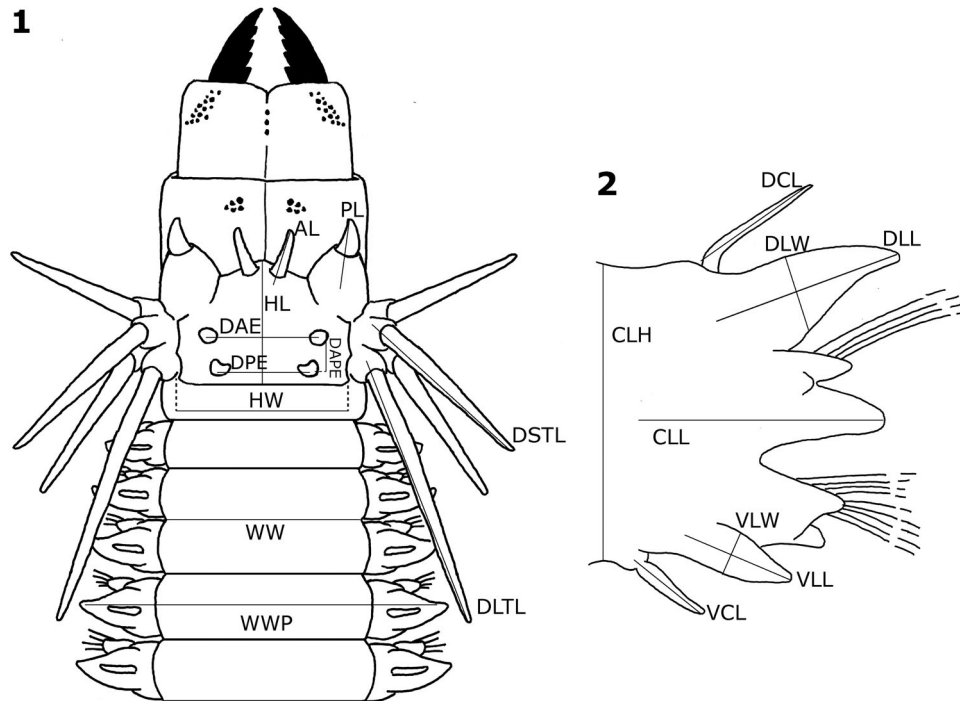
## Genetic diversity and structure

Genetic distances (Kimura-2-parameters, K2P) between all records (for each marker) were calculated using MEGA 10.0.05 and plotted two-dimensionally (multidimensional scaling – mds) using R 3.6.0 software and the package ‘stats’ (function `cmdscale`: distances) (R Core Team, 2019; [www.r-project.org](http://www.r-project.org)). The mean genetic distances (K2P) within and between MOTUs for each individual genetic marker were calculated in MEGA 10.0.05.

Haplotype networks were made for the original sequences through the PopART software (Leigh & Bryant, 2015) using the TCS method (Clement *et al.*, 2002) to evaluate the relationship between the haplotypes and their geographic distribution. No GBlocks were applied in this analysis to avoid underestimating the number of nuclear haplotypes. Indices of genetic diversity, namely number of haplotypes (h), haplotype diversity (hd), polymorphic sites (S), nucleotide diversity ( $\pi$ ), Fu & Li D and Tajima D statistical tests, were estimated based on COI for each MOTU using DNASP 5.10 (Librado & Rozas, 2009).

## Morphometric analysis

Specimens from the different *Hediste* MOTUs (NE Atlantic and Norway; Adriatic Sea; northern Aegean Sea; Sweden and Western Mediterranean) were used for



**Figs 1–2.** Schematic of the *Hediste diversicolor* morphotype showing the measurements used in the morphometric analysis. 1. Anterior end. 2. Parapodia. Abbreviations: the length of the parapodium up to the median ligule (CLL), antennae (AL), palps (PL), antero-dorsal cirri and postero-dorsal cirri (DSTL, DLTL, respectively), dorsal and ventral cirri of median segments (DCL, VCL), dorsal and ventral ligule of median segments (DLL, VLL) and head (HL); the width of the worm with parapodia (WWP) and without parapodia (WW), head (HW), dorsal and ventral ligule (DLW, VLW); and the distance between the anterior eyes (DAE), distance between the posterior eyes (DPE), distance between the anterior and posterior eyes (DAPE) as well the height of the parapodium (CLH).

morphometric analysis and compared against each other to complement the molecular data. A total of 25 specimens with optimal conditions (i.e. specimens with the presence of the proposed morphological characters for this study and whenever possible, similar in size) per MOTU were chosen.

The following characters were selected and measured (Figs 1, 2): the number of chaetigers (NC); the length (mm) of the entire worm (WL), parapodium up to the median ligule (CLL), antennae (AL), palps (PL), antero-dorsal cirri and postero-dorsal cirri (DSTL, DLTL, respectively), dorsal and ventral cirri of median segments (DCL, VCL), dorsal and ventral ligule of median segments (DLL, VLL) and head (HL); the width (mm) of the worm with parapodia (WWP) and without parapodia (WW), head (HW), dorsal and ventral ligule (DLW, VLW); and the distance between the anterior eyes (DAE), distance between the posterior eyes (DPE), distance between the anterior and posterior eyes (DAPE) as well as the height (mm) of the parapodium (CLH). WW, WWP and the different parapodia structures were measured from the worm's widest part, usually from segment 20–45 depending on the worm size.

The distance between the eyes was measured from the centre of the eyespots to avoid possible different individual responses to fixation as in the case of hesionids in Martin et al. (2017). For measuring length of the dorsal ligules, not just the length of their tips were taken into account (e.g. Conde-Vela and Salazar-Vallejo 2015, Villalobos-Guerrero and Carrera-Parra 2015) because dorsal cirri are displaced toward tips of dorsal/notopodial dorsal ligules towards the posterior end. To minimize bias based on size variability, measurements taken to analyse the inter-population differences were converted to ratios and submitted to two types of analysis: (1) taxonomically relevant character proportions through a PCA analysis (i.e. AL/PL, DLTL/DSTL, AL/DLTL, AL/DSTL, PL/DLTL, PL/DSTL, AL/HL, PL/HL, AL/HW, PL/HW, HL/HW, DAE/DPE, DAPE/HL, DAE/HW, DPE/HW, WW/WWP, WL/WW, NS/WW, NS/WL, DCL/VCL, DLL/VLL, DLL/DLW, VLL/VLW, DCL/DLL, CLL/CLH, CLL/VCL, CLL/DCL) and (2) raw data used to create scatter plots between morphological characters with particularly high SIMPER dissimilarity.

Principal Component Analysis (PCA) was based on normalized data. The significance of the inter-population

differences was explored by one-way analysis of similarity (ANOSIM) based on Euclidean distance resemblance matrices. The contribution of each measured character to the distance within and between the four species was assessed by the Similarity Percentages analysis (SIMPER) based on Euclidean distance. Both SIMPER and ANOSIM also used the normalized proportion dataset and were conducted using Primer-E software Version 6.1.11 (Clarke & Warwick, 2001; Gorley & Clarke, 2006). All measurements were done with a Leica MC170HD stereo microscope, with an incorporated measurement software. [Supplemental Table S3](#) shows detailed morphometric values for each specimen.

### Morphological analysis

For analysis of variation, both complete and incomplete specimens were taken into account, with incomplete specimens lacking a very small part of the tissue in the posterior end due to sampling techniques or use for molecular purposes; total length (TL), length up to chaetiger 15 (L15), width at chaetiger 15 (W15) were measured with a millimetre rule under the stereomicroscope, number of chaetigers (NC) was included. TL was measured from anterior margin of prostomium to the end of the pygidium or the posterior end, and W15 were measured excluding parapodia. Further measurements were also recorded for the different structures within the parapodia (antennae, palps and tentacular cirri).

Representative specimens from each *Hediste* lineage were used for scanning electron microscopy (SEM). These specimens were transferred to 100% ethanol, dehydrated for 2 hours with hexamethyldisilazane (HMDS,  $\geq 99\%$ ) and left to dry overnight. No coating was applied. Images were obtained using a TM3030Plus tabletop microscope (Hitachi). Morphological observations were carried out with an Olympus stereo microscope equipped with a camera lucida for line drawings. Stereo microscope images were taken with a Canon EOS1100D camera. Compound microscope images of parapodia and chaetae were obtained with a Zeiss Axioplan 2 imaging light microscope (Carl Zeiss, Oberkochen, Germany), equipped with a DP70 Olympus camera (Olympus Corp., Tokyo, Japan), after mounting the parapodia on a slide preparation using Aquamount (Gurr) liquid. The software Inkscape 0.92.3 (<https://www.inkscape.org>) was used to create the final images for the drawings of the parapodia.

Terminology for molecular vouchers follow Pleijel *et al.* (2008) and Astrin *et al.* (2013). Overall description from the taxonomic section follows a similar structure from Villalobos-Guerrero (2019) in line with other recent descriptions of nereidid species. Parapodial and

chaetal terminology in the taxonomic section follows Bakken and Wilson (2005) with the modifications made by Villalobos-Guerrero and Bakken (2018). Pharynx paragnath terminology follows Bakken *et al.* (2009).

## Results

### Phylogenetic reconstruction

The concatenated BI tree (Figs 3, 4) shows evidence of at least five different species belonging to the *Hediste diversicolor* complex. There is a MOTU consensus, corresponding to each of the monophyletic clades with low divergence, belonging to MOTU 1, MOTU 3, MOTU 4 and MOTU 5. However, none of the species delineation methods or the morphometric data provided by the PCA and SIMPER analysis, reached a consensus to define the previously defined ‘Species A’ as a single entity. This massive clade varied between 1–35 MOTUs and has genetic distances above 3%, reaching almost 7% in two of the four sub-clades present in the BI tree. The bPTP method grouped all the *Hediste* populations into a single entity and the PCA grouped MOTUs 1 and 2 together. To achieve consensus as MOTU 2 corresponding to Species A, the most conservative result within the major clade was chosen (SIMPER).

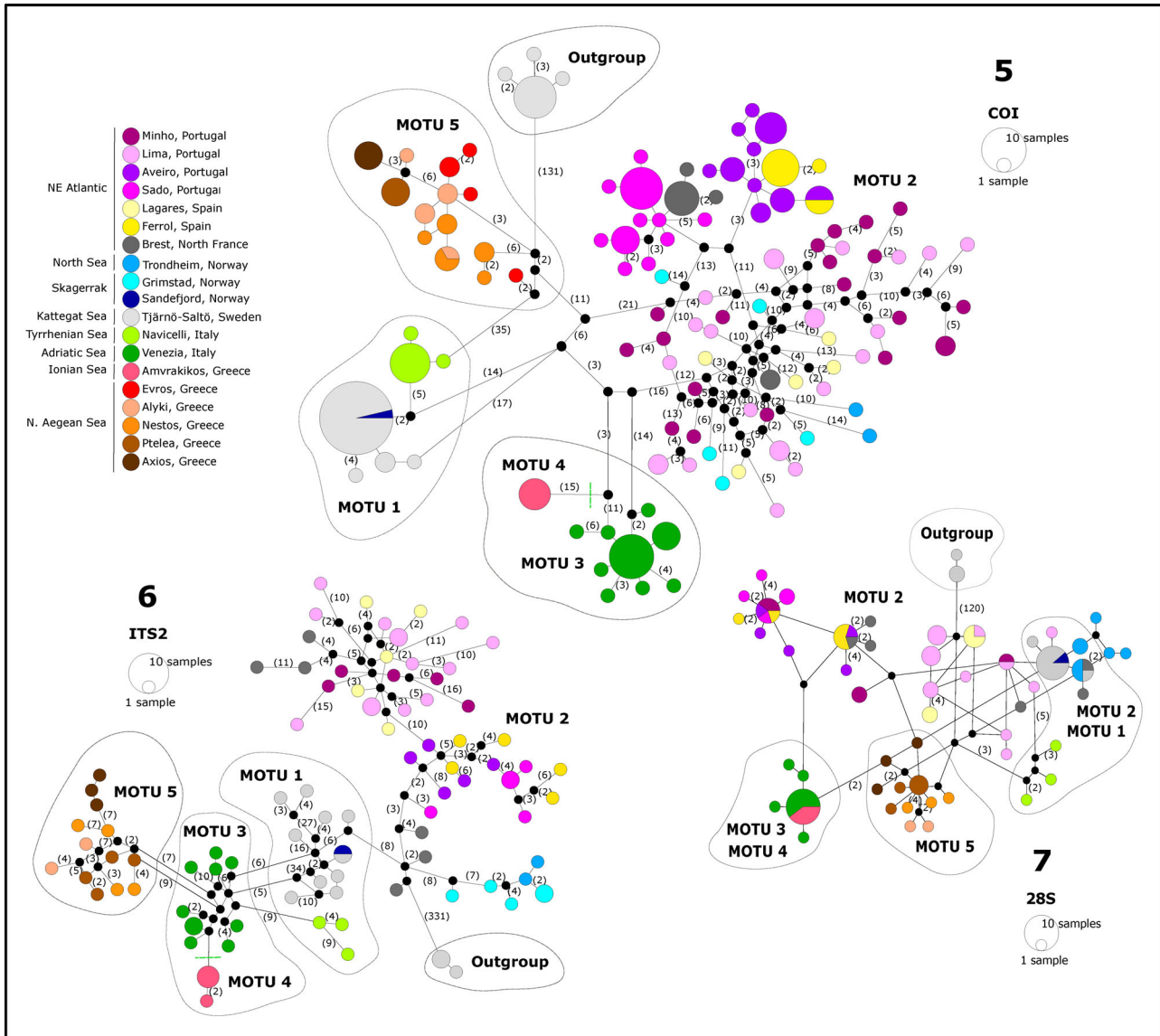
The phylogeographic structure of the European *Hediste diversicolor* comprises at least four divergent lineages (Fig. 4). MOTU 1 occurs in the western part of the Mediterranean (Tyrrhenian Sea), north-east Skagerrak, Kattegat Sea and in the Baltic Sea. MOTU 2 can be found in all of the NE Atlantic and Scandinavia, ranging from Portugal and Morocco to Norway (excluding the north-eastern part of the Skagerrak), French part of the Western Mediterranean (based on a *cytb* sequence from Breton *et al.* (2003)), and also in the Baltic Sea in sympatry with two other lineages (MOTUs 1 and 5). The *cytb* sequence grouped in the same clade as the COI sequences from Virgilio *et al.* (2009), which in turn corresponds to the clade identified as MOTU 2 in this study. MOTU 3 is exclusive to the Adriatic Sea, biogeographically part of the eastern Mediterranean, while MOTU 4 is present only in Greece in the Ionian Sea. Lastly, MOTU 5 is located in eastern Greece (northern Aegean Sea) and corresponds to the same MOTU found in the Caspian and Black Sea from previous studies.

A non-collapsed ML tree with 1000 bootstrap support for the concatenated dataset can be seen in the [Supplemental Fig. S1](#).

### Haplotype networks

The COI (Fig. 5) and ITS2 (Fig. 6) haplotypes completely sorted all MOTUs, and no haplotype has a





**Figs 5–7.** Haplotype networks for COI (5), ITS2 (6) and 28S (7) for all the five MOTUs based on the original *Hediste* data and *Alitta virens* as outgroup. Each haplotype is represented by a circle and number of haplotypes are according to the displayed scale. Colours indicate the geographic location of the haplotype. Numbers correspond to the number of mutational steps between haplotypes. Lines without numbers means only one mutation between haplotypes.

**Table 4.** For COI, the mean intraspecific distance is 1.13% (0.0–7.5), while the average congeneric distance is 6.9% (4.1–10.1). For the ITS2-region it ranges between 2.6% (0.0–10) and 4.6% (0.3–11.6) for intra- and interspecific divergence, respectively, while for 28S the corresponding distances are 0.5% (0–1.7) and 0.7% (0–2.4), respectively. MOTUs 3 and 4 have low genetic divergence between them, with just 4.4% COI and 1.4% ITS2 genetic distances (K2P), which is lower than the intraspecific divergence found within MOTU 2. The latter shows unusual high genetic distances within populations of the same estuary as

seen in Table 3. These high genetic distances are present in the estuaries of Lima, Minho, Lagares and in the Norwegian specimens, where the number of BINs and haplotypes are unusually high as well. The Lima Estuary in particular not only has maximum COI distances reaching almost 7%, but also has 17 BINs, with 8 of them being unique to the estuary and the remaining 9 being shared with populations from Minho and Lagares (Table 3). In contrast, *Hediste* populations from the estuaries of Sado, Aveiro and Ferrol, also from MOTU 2, have less than 1.5% intraspecific COI divergence, with the Brest population having a mixed

**Table 2.** Indices of genetic diversity estimated for each MOTU, based on COI and from the original data.

	Region	N	h	Hd	S	$\pi$	Fu and Li's D	Tajima's D
MOTU 1	NV, TJ, SF	41	7	0.54	15	0.005	-1.48049 P > 0.10	-0.34310 P > 0.10
MOTU 2	SA, AV, FE, BR, GM, TD, LI, MI, LA	117	77	0.98	190	0.035	-2.21398 0.10 > P > 0.05	-1.51333 P > 0.10
MOTU 3	VE	21	9	0.76	20	0.003	<b>-3.30826</b> P < 0.02	<b>-2.25699</b> P < 0.01
MOTU 4	AM	5	1	0	0	0	-	-
MOTU 5	NAS	27	14	0.94	32	0.012	0.12419 P > 0.10	-0.31253 P > 0.10

Number of sequences (n); nucleotide diversity ( $\pi$ ), number of haplotypes (h), haplotype diversity (Hd) and number of variable sites (S). Region abbreviations as stated in Table 1. Values in bold are statistically significant.

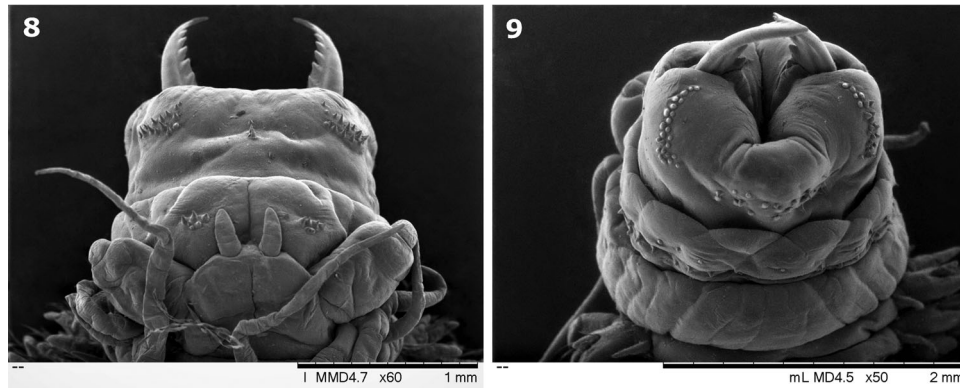
**Table 3.** Haplotypes, number of BINs and genetic distances (COI) comparisons within the different populations from the five retrieved MOTUs, based on the original data.

	Populations	n	h	Hd	BINs (shared)	Mean Distance (%)	Maximum distance (%)
MOTU 1	Tjärnö	30	4	0.251	1	0.1	0.9
	Navicelli	10	3	0.378		0.1	0.3
MOTU 2	Minho	20	19	0.995	<b>6 (7)</b>	<b>4.1</b>	<b>6.9</b>
	Lima	23	19	0.984	<b>8 (9)</b>	<b>4.5</b>	<b>6.8</b>
	Lagares	5	5	1	<b>3 (2)</b>	<b>3.2</b>	<b>4.4</b>
	Grimstad	5	5	1	<b>5</b>	<b>4.6</b>	<b>6.4</b>
	Trondheim	2	2	1	<b>2</b>	<b>4.4</b>	<b>4.4</b>
	Aveiro	20	10	0.905	<b>1</b>	0.5	1.1
	Sado	22	11	0.818	<b>1</b>	0.5	1.4
	Brest	10	4	0.644	<b>1 (1)</b>	1.3	3.6
	Ferrol	10	3	0.511	<b>1</b>	0.3	0.9
MOTU 3	Adriatic Sea	21	9	0.757	1	0.3	1.7
MOTU 4	Amvrakikos	5	1	0	1	0.0	0.0
MOTU 5	N. Aegean Sea	27	14	0.943	1	1.2	3.1

Values in bold are unusual, with high haplotype diversity, as well as with more than 3.5% COI distances. Coloured values with the same colour share the same BIN.

**Table 4.** Mean intra (in bold) and inter-MOTU genetic distances (K2P) for the three analysed markers (COI, ITS2, 28S), for the five retrieved *Hediste* MOTUs, based on the original data.

	Loci	1	2	3	4	5
MOTU 1 (Species B1)	COI	<b>0.5±0.4</b>				
	ITS2	<b>4.8±0.4</b>				
	28S	<b>0.6±0.2</b>				
MOTU 2 (Species A)	COI	7.8±0.9	<b>3.6±0.2</b>			
	ITS2	6.5±0.6	<b>4.3±0.5</b>			
	28S	0.8±0.2	<b>0.8±0.2</b>			
MOTU 3 (Species B2)	COI	5.7±0.9	7.5±0.9	<b>0.3±0.1</b>		
	ITS2	4.6±0.5	5.4±0.6	<b>1.8±0.3</b>		
	28S	0.9±0.2	0.7±0.2	<b>0.2±0.1</b>		
MOTU 4 (Species B3)	COI	6.1±0.9	7.8±0.9	4.4±0.8	<b>0.0±0.0</b>	
	ITS2	4.3±0.6	4.9±0.6	1.4±0.3	<b>0.1±0.1</b>	
	28S	0.9±0.2	0.7±0.2	0.1±0.0	<b>0.0±0.0</b>	
MOTU 5 (Species B4)	COI	7.0±1.0	8.2±0.9	7.3±1.0	7.7±1.0	<b>1.2±0.2</b>
	ITS2	5.9±0.7	6.7±0.8	3.5±0.5	2.8±0.5	<b>1.7±0.3</b>
	28S	0.8±0.2	0.8±0.2	0.7±0.2	0.6±0.2	<b>0.4±0.1</b>



**Figs 8–9.** Representative SEM images for paragnath patterns found in the *Hediste diversicolor* species complex. 8. Paragnath patterns in the worm’s pharynx, dorsal view (specimen DBUA0002466.05.v01). 9. Paragnath patterns in the worm’s pharynx, ventral view (specimen DBUA0002466.05.v01).

genetic variation corresponding to the two different BINs.

No genetic structure (i.e. genetic populations sorted geographically) seems to be patent within MOTU2 (Supplemental Fig. S3).

## Morphology

All four analysed MOTUs failed to provide consistent morphological differences between specimens from the different MOTUs. The paragnath patterns present in the worm’s pharynx (Figs 8, 9) are consistent with the descriptions of *H. diversicolor* (Müller, 1776) with some variation in the numbers found between the MOTUs. The low number of paragnaths in MOTUs 3 and 5 (detailed in the taxonomic section, Table 5), especially in areas III and IV, can sometimes reach half the number as the ones found in MOTU 2 and may be a diagnostic feature, but phenotypic variation is high among the specimens. The chaetae types and respective distribution throughout the body were also similar among all the analysed lineages, but different when compared with Asiatic *Hediste* species (Table 5) and are further detailed in the taxonomic section for each of the three described lineages (MOTUs 2, 3 and 5): Homogomph spinigers with blades coarsely serrated, evenly spaced, present in notopodia and neuropodial supracircular fascicles. Heterogomph and homogomph spinigers, present in neuropodial supracircular and subacircular fascicle. Heterogomph falcigers with long blades, present in both neuropodial fascicles. One large fused falciger present in the neuropodial supracircular fascicle in the posteriormost chaetigers. Spinigers more numerous than falcigers throughout the body. However, in MOTU 5, falciger numbers are apparently higher than spinigers in the neuropodial subacircular fascicle from the anterior and median parapodia. No major differences

were found in parapodia structures between the four analysed MOTUs (Figs 10–21), with the complex having thick dorsal ligules longer and wider than ventral ligules and dorsal cirri longer than ventral cirri, both with at least half the size of the respective ligules. However, the proportions between the parapodial structures throughout the body seem to differ for the different MOTUs and together with measurements of the head appendages and eyes, were further explored using morphometric data.

## Morphometry

The morphometric proportion data in the PCA analysis individualized three distinct clusters corresponding to the combined data between MOTU 1/MOTU 2 against MOTU 3 and MOTU 5, segregating them into three clear groups (Fig. 22). Photos from preserved specimens belonging to MOTU 3 and MOTU 5 can be seen in Fig. 23 and Fig. 24, respectively. Morphometric measurements from the specimens belonging to MOTUs 1 and 2 are scattered and overlapping, failing to produce two separated groups. Specimens from both the western Mediterranean and Sweden were used in MOTU 1, while Norwegian and Portuguese samples (mainly from Minho and Sado) were used for the measurements in MOTU 2. No significant differences were found between and within these populations. Twenty-seven character proportions were used in the PCA discrimination, with Axes 1 (eigenvalue = 9.18) and 2 (eigenvalue = 4.55) explaining 34.0% and 16.9% of the variation, respectively. The ANOSIM test indicates significant differences between the morphometric data of the four analysed MOTUs (Global R = 0.756; significance level at 0.1%).

The average morphometric variation within species provided by the SIMPER results is 17.51% for MOTU

**Table 5.** Comparison between the described lineages within the *Hediste diversicolor* species complex and against the closely related Asiatic *Hediste* species (Sato & Nakashima, 2003; *H. japonica*, *H. atoka* and *H. diadroma*).

Morphological features	Species					
	<i>H. japonica</i>	<i>H. atoka</i>	<i>H. diadroma</i>	<i>H. diversicolor</i> MOTU 2	<i>H. pontii</i> sp. nov. MOTU 3	<i>H. astae</i> sp. nov. MOTU 5
Chaetae						
Heterogomph spinigers	<b>Absent in neuropodia</b>	Present in NsubF (less numerous than falcigers)	Present in NsubF (less numerous than falcigers)	Present in NsubF (more numerous than falcigers)	Present in NsubF (more numerous than falcigers)	Present in NsubF (less numerous than falcigers)
Homogomph spiniger	Present in Noto and NsubF	Present in Noto, NsubF and NsubF	Present in Noto, NsubF and NsubF	Present in Noto and NsubF	Present in Noto and NsubF	Present in Noto and NsubF
Heterogomph falciger	Present in NsubF and NsubF	Present in NsubF and NsubF	Present in NsubF and NsubF	Present in NsubF and NsubF	Present in NsubF and NsubF	Present in NsubF and NsubF
Homogomph falciger	<b>Present in NsubF</b>	Absent	Absent	Absent	Absent	Absent
Fused falciger	Present	Present	Present	Present	Present	Present
Paragnath numbers	(posterior most chaetigers)	(posterior most chaetigers)	(posterior most chaetigers)	(posterior most chaetigers)	(posterior most chaetigers)	(posterior most chaetigers)
Area I	1-4	0-8	1-8	2-6	1-3	1-2
Area II (single side)	< 10-11	21	15-16	9-23	10-17	5-15
Area III	23-30	23-79	22-61	24-52	22-25	19-29
Area IV (single side)	10-11	25-26	24	19-38	17-20	13-22
Area V	absent	absent	absent	absent	absent	absent
Area VI (one side)	5-8	5-6	6	3-8	3-8	3-8
Area VII-VIII	19-26	9-35	11-41	30-38;	30-36;	22-30;
Number of denticles per half jaw	8-9	7-9	6-9	6-8	9-10	7-8
Reproduction	Swarming. No epitokous form. 10-day planktic trochophore/nectochaeta. Eggs 180-210	<b>Female spawns in burrow. No epitokous form. No planktonic larvae. Eggs 200-250</b>	<b>Swarming. Epitoke-specific sesquigomph spinigers. Eggs &lt;170 mm diameter</b>	Anterior row with double the number of the posterior one	Anterior row with double the number of the posterior one	<b>Two tight rows with subequal numbers</b>
Distribution	The coasts of the Yellow Sea in Korea, the Seto Inland Sea and Ariake Sea in Japan	The coasts of Japan	The coasts of Japan and China	Female spawns, broods embryos in burrow. No epitokous form. 10-week demersal trochophore/nectochaeta. Eggs 200-250	<b>Adriatic Sea (E Mediterranean Sea)</b>	<b>Aegean, Black, Caspian and Baltic Seas</b>
				<b>NE and NW Atlantic coasts, Baltic Sea, W Mediterranean Sea</b>		

(continued)

Table 5. Continued.

Morphological features	Species					
	<i>H. japonica</i>	<i>H. atoka</i>	<i>H. diadroma</i>	<i>H. diversicolor</i> MOTU 2	<i>H. pontii</i> sp. nov. MOTU 3	<i>H. astae</i> sp. nov. MOTU 5
Colouration in preserved specimens	Whitish cream, with dark brown pigmentation on the anterior dorsal surface	Whitish cream, with dark brown pigmentation on anterior dorsal surface	Whitish cream, with dark brown pigmentation on anterior dorsal surface	Blood vessel often visible. Yellowish-green or yellowish brown	Blood vessel often absent. Yellowish-brown	Blood vessel often absent. Yellowish-brown or orange-brown
Observations based on chaetae types, paragnath numbers, number of denticles per half jaw, colouration in preserved specimens, geographic distribution and known reproductive history. Features in bold show considerable differences. Abbreviations: NsuBF, Neuropodial subacicular fascicle; NsuPF, Neuropodial supracicular fascicle; Noto, Notopodium.						

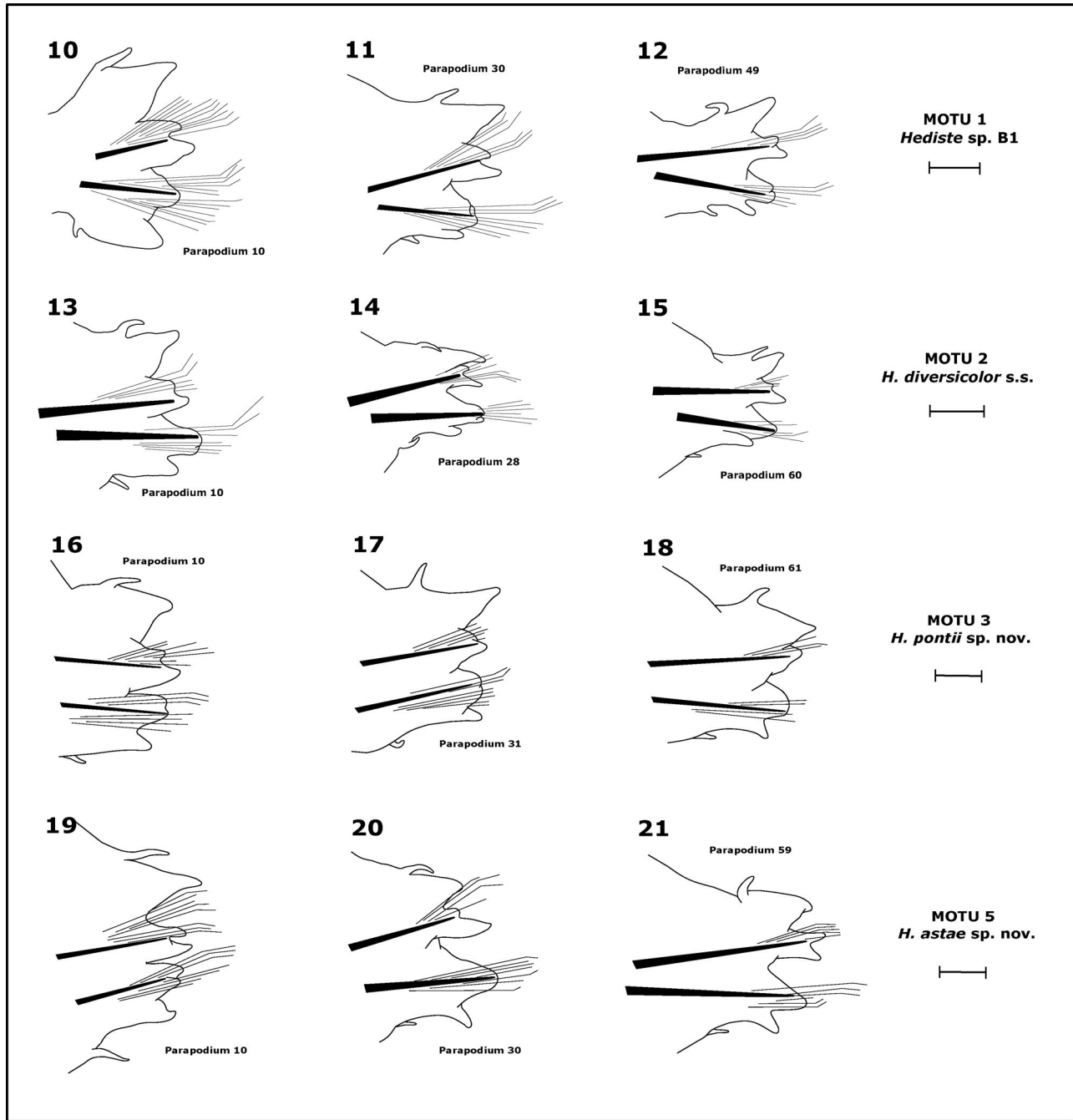
2, 11.90% for both MOTU 1 and MOTU 3 and 16.37% for MOTU 5. The average inter-species distance ranges between 37.64% (MOTU 1/MOTU 2) and 91.47% (MOTU 3/MOTU 5), with greater distances when involving MOTU 5 (Table 5). The three most significant proportions for the inter-species dissimilarity are summarized in Table 6, all with more than 4.50% of contribution. The length and width of the head (HL, HW), head appendages (AL, PL, DLTL, DSTL) and distance between the posterior eyes (DPE) are the features that, when combined, most contributed to the divergence between all the analysed lineages. Worm width and length (WW and WL, respectively) and number of chaetigers (NC) are also highlighted when comparing MOTU 2 against MOTU 3, and MOTU 3 with MOTU 5.

Traditional morphometric approaches based on scatter plots by using relevant combinations of the most significant characters revealed by the SIMPER analysis (the length of the antennae against either the length of the head, the antero-dorsal cirri and postero-dorsal cirri), have enough divergence to display two partial clusters for each of the analysed lineages as seen in Figs 25–27. These are the only combinations with distinct clusters between MOTUs 1 and 2, which explain the PCA result and low inter-species morphometric distance reported above. Excluding MOTU 1, a summary was done in Table 7 based on morphometric ratios and observation of the scatter plots between the lineages that properly segregated in the PCA analysis (Figs 28–35). The proportions DLTL/DSTL, DLTL/WW, DSTL/PL, HL/AL, PL/AL, DAE/DPE and DLL/DCL were used to further differentiate between MOTUs and complement the taxonomic description.

## Taxonomic section

### *Hediste diversicolor* species complex.

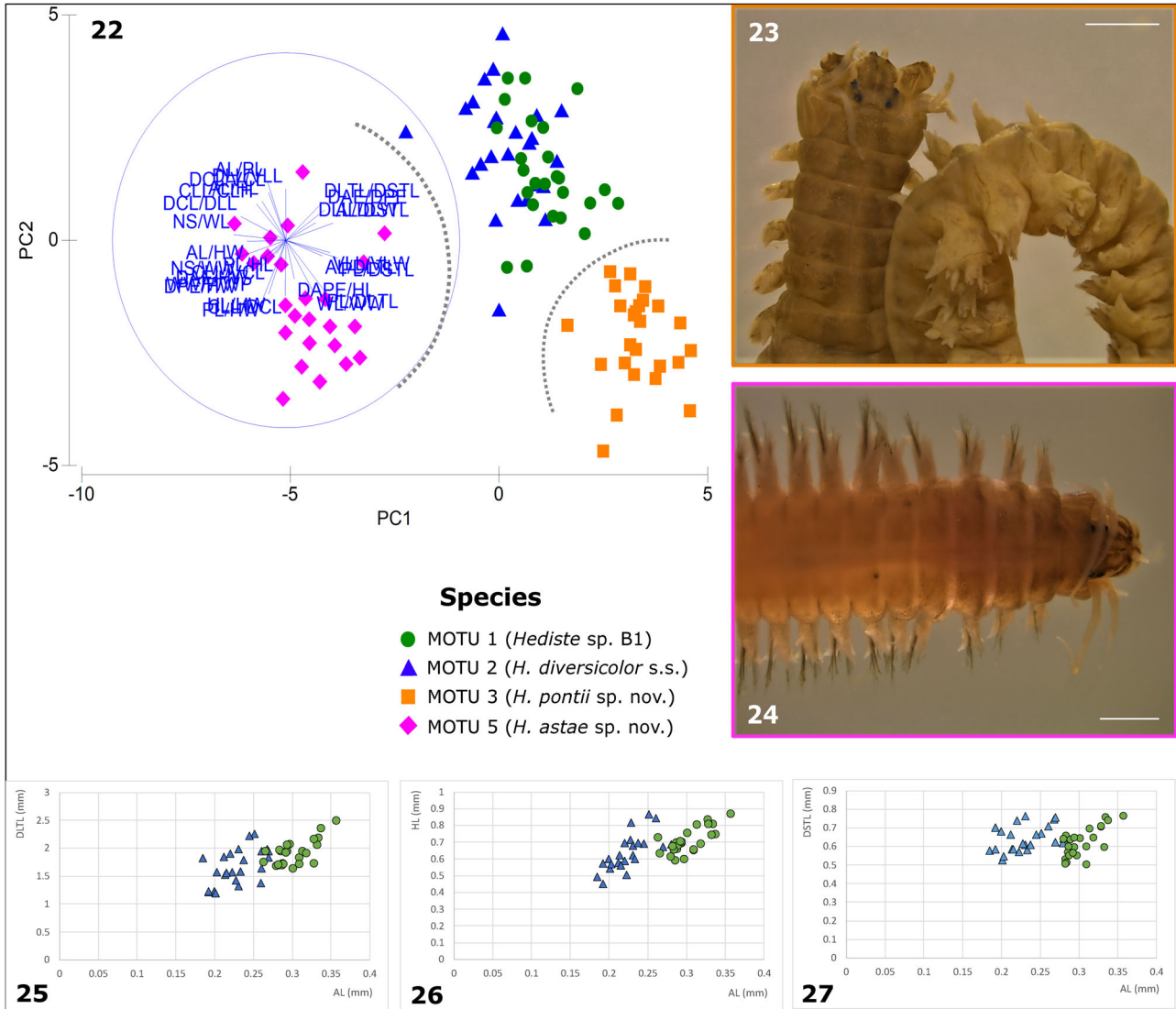
**Diagnosis.** Body may have a prominent dorsal blood vessel; small to large-sized worm stout anteriorly, posteriorly gradually tapering toward pygidium. Around 40–100 chaetigers. Colour variable between yellow-greenish, yellowish-brown or orange-brown in preserved specimens. Head pyriform wider than long; 2.5–3 times longer than antennae. Palpophore 2–2.5 times longer than the antennae. Distance between the anterior eyes subequal to 1.3 times longer than the posterior ones. Postero-dorsal cirri as long as body width or shorter, reaching chaetiger 2–6. Nuchal organs deeply embedded, transverse, usually wider than posterior eyes. Pharynx consisting of maxillary and oral ring with conical paragnaths (Figs 8, 9): Area I with small number of paragnaths forming a longitudinal line or a shapeless



**Figs 10–21.** Drawings of the main morphological features found in the parapodia from different parts of the worm's body. Scale bars = 0.5 mm. MOTU 1 (*Hediste* sp. B1, specimen DBUA0002463.02.v06): 10. Parapodium 10, posterior view. 11. Parapod 30, posterior view. 12. Parapodium 49, posterior view; MOTU 2 (*Hediste diversicolor* s.s., specimen DBUA0002460.02.v06): 13. Parapodium 10, posterior view. 14. Parapodium 28, posterior view. 15. Parapodium 60, posterior view; MOTU 3 (*Hediste pontii* sp. nov., specimen DBUA0002465.02.v01): 16. Parapodium 10, posterior view. 17. Parapodium 31, posterior view. 18. Parapodium 61, posterior view; MOTU 5 (*Hediste astae* sp. nov., specimen DBUA0002466.02.v05): 19. Parapodium 10, posterior view. 20. Parapodium 30, posterior view. 21. Parapodium 59, posterior view.

group. Area II with paragnaths forming a diagonal thick line. Area III with large number of paragnaths in a transverse band. Area IV with large number of

paragnaths in arched rows, forming a 'C' shape group in the left side; inverted 'C' in the right one. Area V absent. Area VI with paragnaths arranged in small



**Figs 22–27.** Principal Component Analysis (PCA) plots based on proportion data. 22. Plot between MOTUs 1, 2, 3 and 5. Twenty-seven character proportions were used, as listed in the methods. 23. Scale bar = 2 mm. Photo of a preserved specimen from MOTU 3 (DBUA0002465.01.v01). 24. Scale bar = 500  $\mu$ m Photo of a preserved specimen from MOTU 5 (DBUA0002466.07.v04); Scatter plots with the most significant proportions in distinguishing MOTU 2 (*Hediste diversicolor* s.s.) from MOTU 1 (*Hediste* sp. B1). 25. Measurements between the length of the antennae (AL) and the length of the postero-dorsal cirri (DLTL). 26. Measurements between the length of the antennae (AL) and the length of head (HL). 27. Measurements between the length of the antennae (AL) and the length of the antero-dorsal cirri (DSTL).

clusters in each side. Area VII–VIII with two bands of paragnaths. Pair of dark brown jaws, each with 6–10 denticles; 2 longitudinal canals emerging from pulp cavity, both closer to the inner edge. Dorsal cirri shorter than dorsal ligule throughout the body; proportion ratio variable throughout the body. Ventral cirri shorter than ventral ligule throughout the body; proportion ratio variable throughout the body. Proportion ratio between notopodial prechaetal lobe and median ligule variable throughout the body. Neuropodial postchaetal lobe well developed in anterior parapodia, gradually diminishing

in size towards mid-body, hardly distinguishable posteriorly. Homogomph spinigers with blades coarsely serrated, evenly spaced; present in notopodia and neuropodial supracicular fascicles. Heterogomph spinigers as homogomph ones; present in neuropodial supracicular and subacicular fascicle. Heterogomph falcigers with long blades, present in both neuropodial fascicles. One large fused falciger present in the neuropodial supracicular fascicle in the posteriormost chaetigers. Spinigers more numerous than falcigers throughout the body. Falciger numbers may sometimes

**Table 6.** List of the three most contributing proportions to the inter-population dissimilarities based on the SIMPER analyses.

	Proportions	Contribution (%)	Ratio	Average Inter-variation (%)	ANOSIM
MOTUs 2 vs 1	AL/DLTL	5.43	MOTU 1 > AL; similar DLTL, DSTL and HL	37.64	0.376 at 0.1%
	AL/DSTL	5.37			
	AL/HL	4.54			
MOTUs 2 vs 3	DLL/VLL	7.16	MOTU 3 > proportions	58.08	0.752 at 0.1%
	WL/WW	7.10			
	CLL/CLH	7.00			
MOTUs 2 vs 5	WW/WWP	7.28	MOTU 5 < proportions	69.86	0.858 at 0.1%
	DPE/HW	6.54			
	PL/HW	6.04			
MOTUs 1 vs 3	AL/HL	8.66	MOTU 3 > HL, PL but similar AL; > DAPE/HL	44.84	0.744 at 0.1%
	AL/PL	8.52			
	DAPE/HL	7.65			
MOTUs 1 vs 5	DLTL/DSTL	7.94	MOTU 5 < proportions	71.12	0.946 at 0.1%
	AL/DSTL	7.83			
	DPE/HW	6.28			
MOTUs 3 vs 5	NC/WL	7.46	MOTU 3 > proportions	91.47	0.961 at 0.1%
	PL/DSTL	6.92			
	NC/WW	6.15			

be higher than spinigers in the neuropodial subaciclar fascicle from the anterior and median parapodia. Geographic distribution ranging from the NE and NW Atlantic coasts to the Mediterranean and Baltic, Black and Caspian Seas.

**Remarks.** The detailed description of three, from the five European lineages belonging to the *H. diversicolor* complex are provided below, namely for: *H. diversicolor* s.s., *H. pontii* sp. nov. and *H. astae* sp. nov. The two remaining lineages (*Hediste* sp. B1 and *Hediste* sp. B3) stay unnamed; the former due to possible hybridization with *H. diversicolor* s.s in the Baltic Sea, requiring further reproductive and ecological data to clarify its taxonomic status and the latter for currently only having molecular data available, lacking available specimens to test possible morphological and morphometric variations in this study. Nevertheless, both molecular and geographic distribution data associated with these unnamed MOTUs provide a great starting point for future research (Tables 1, Supplemental Table S1 and Figs 3, 4).

The presence of a simple straight fused falciger in the posterior neuropodia is the most important diagnostic characteristic separating *Hediste* from *Nereis* and *Neanthes* (Bakken & Wilson, 2005; Sato & Nakashima, 2003). *Hediste* species, however, are morphologically very similar; for example when comparing Asian *Hediste* species (*H. japonica* (Izuka, 1908), *H. atoka* Sato & Nakashima, 2003 and *H. diadroma* Sato & Nakashima, 2003) between each other or against the European *H. diversicolor*, besides reproductive and geographic distribution data, the variation is mainly found in chaetae types, including their position in the

parapodia and respective numbers (Table 5). Paragnath numbers may be a diagnostic feature, however phenotypic variation is high between and within species (Table 5). This close morphological similarity is mirrored by the molecular data, where phylogenetic analysis and genetic distances based on commonly used markers (COI, 16S, 28S) reveal a closely related complex (Tosuji et al., 2019). These low genetic distances (e.g. in the DNA barcode gene COI) between species also characterize the different MOTUs found within the *Hediste diversicolor* species complex from our study, which are within the lower boundaries (max. divergence up to 10.1%) when compared with other polychaete works (>15%, Carr et al., 2011; Lobo et al., 2016; Ravara et al., 2017; Sampieri et al., 2021). At the same time, *H. diversicolor* s.s. is also characterized by the unusual high number of BINs, haplotype numbers and within-clade COI genetic distances (up to 7.5%, Table 4), which is much higher than what is usually observed within species clades (<3%, Glasby, 2005; Paiva et al., 2019; Teixeira et al., 2022). These high haplotype numbers and intraspecific genetic distances can also be found in *H. atoka* to a lesser degree, which has at least two molecular forms (Forms A and B; Tosuji et al., 2019).

Simple Key to the three European *Hediste* species described in this study

1. Falciger chaetae more numerous than spinigers in the neuropodial subaciclar fascicle from the anterior and median parapodia; subequal values between the distance of the anterior (may be slightly longer) and posterior eyes ... .. *H. astae* sp. nov. – Spiniger chaetae more numerous than falcigers

**Table 7.** Observations based on morphometric ratios between the three described species (*H. diversicolor* s.s., *H. pontii* sp. nov. and *H. astae* sp. nov.).

Morphometric ratios	Species		
	<i>H. diversicolor</i> MOTU 2	<i>H. pontii</i> sp. nov. MOTU 3	<i>H. astae</i> sp. nov. MOTU 5
Mean NC / WW (median body) / WL	63 / 1.6 / 27.2	78 / 2.4 / 65.6 <b>Much larger worms, but often relatively close number of chaetigers to MOTUs 2 and 5 in some specimens (Figs 28, 29)</b>	58 / 0.8 / 15.2
DLTL / DSTL	1.7 – 2.6 x; DLTL reaching chaetiger 4–5, DSTL reaching chaetiger 2–3.	1.5 – 2.7 x; DLTL reaching chaetiger 2–3, DSTL reaching chaetiger 1–2.	1.4 – 2 x; DLTL reaching chaetiger 4–6, DSTL reaching chaetiger 2–4; <b>Much smaller worm, but subequal DSTL values as MOTU 2 (Fig. 32)</b>
DLTL / WW (median body)	< 1.1 x	<b>0.75 x;</b> Much larger worm, but similar DLTL values as MOTU 2 (Fig. 30)	<1.4 x; <b>Much smaller worm, but subequal DLTL values in some specimens as MOTU 2 (Fig. 30)</b>
DSTL / PL	1.3 x	1–1.4 x; Much larger worm, but similar DSTL values as MOTUs 2 and 5 (Fig. 31)	1.7–2 x; <b>Much smaller worm, but subequal to larger DSTL values as MOTUs 2 and 3 (Fig. 31)</b>
HL / AL	2.7 x	<b>3.1 – 3.2 x</b>	2.5 x
PL / AL	2 x	<b>2.4 – 2.5 x</b>	2 x
DAE / DPE	1.3 x	1.3 x	<b>1.1 x;</b> <b>Subequal values between the distance of the anterior and posterior eyes (Fig. 33)</b>
DLL / DCL (total variation)	1.8 – 3 x; <b>DCL much shorter in median parapodia (3 x)</b>	2.1 – 3 x; DCL gradually diminishing in size throughout the body. Much larger worm, but similar DCL values in median parapodia as MOTU 2 (Fig. 34)	1.4 – 2.6 x; DCL gradually diminishing in size throughout the body.
VLL / VCL (total variation)	1.4 – 3.3 x; <b>VCL much shorter in posterior parapodia (3 x)</b>	1.7 – 2.6 x; <b>VCL much shorter in anterior and median parapodia (2.6 x);</b> Much larger worm, but similar VCL values in median parapodia as MOTU 2 (Fig. 35)	1.2 – 2 x; <b>VCL much shorter in median and posterior parapodia (2 x)</b>

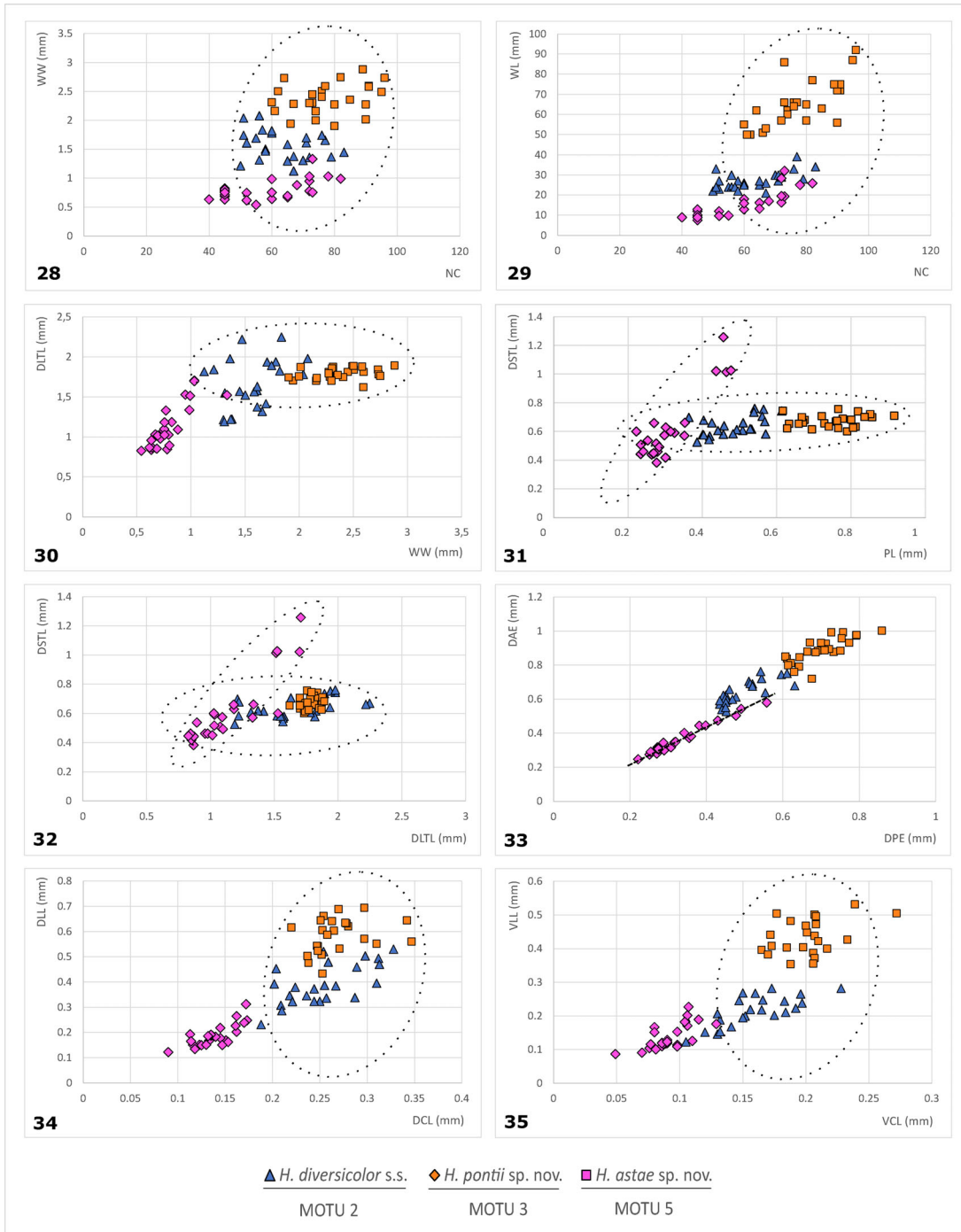
Morphometric proportions: WW, worm width; WL, worm length; NC, number of chaetigers; HL, Head length; AL, antenna length; PL, palp length; DLTL, length of the postero-dorsal cirri; DSTL, length of the antero-dorsal cirri; DCL, length of the dorsal cirri; DLL, length of the dorsal ligule; VCL, length of the ventral cirri; VLL, length of the ventral ligule. Features in bold show considerable differences. Mean WW and WL values in mm.

throughout the whole body; distance of the anterior eyes 1.3 times of the posterior ones .....2  
2(1). Postero-dorsal cirri clearly shorter than body width in median body (<0.75 ratio), reaching chaetiger 2 – 3; dorsal cirri shorter than dorsal ligule, gradually diminishing in size throughout the body; notopodial prechaetal lobe longer than median ligule in posterior parapodia..... *H. pontii* sp. nov.  
– Postero-dorsal cirri slightly longer than body width or slightly shorter, reaching chaetiger 4 – 5; dorsal cirri shorter than dorsal ligule throughout the body, much shorter in median parapodia (three times); notopodial

prechaetal lobe shorter than median ligule throughout the body.....*H. diversicolor* s.s.  
(may be confused with *Hediste* sp. B1 in the Baltic Sea and W Mediterranean; clear distinction between these two lineages only possible with molecular data)

*Hediste diversicolor* (O.F. Müller, 1776) s.s.  
(Figs 13–15, 36–44)

*Nereis diversicolor* O.F. Müller, 1776: 217. – Fauvel 1923: 344,  
fig. 133a–f. – Augener 1933: 247. – Chambers & Garwood 1992: 28–31, fig. 41.



**Figs 28–35.** Scatter plots with the most considerable proportions in distinguishing between MOTUs 2 (*H. diversicolor* s.s.), 3 (*H. pontii* sp. nov.) and 5 (*H. astae* sp. nov.). 28. Measurements between the width of the worm (WW) and the number of chaetigers (NC). 29. Measurements between the length of the worm (WL) and the number of chaetigers (NC). 30. Measurements between the length of the postero-dorsal cirri (DTL) and the width of the worm (WW). 31. Measurements between the length of the antero-dorsal cirri (DSTL) and the length of the palps (PL). 32. Measurements between the length of the postero-dorsal cirri (DTL) and the length of antero-dorsal cirri (DSTL). 33. Measurements between the distance of the anterior eyes (DAE) and the distance of the posterior eyes (DPE). 34. Measurements between the length of the dorsal ligule (DLL) and the length of the dorsal cirri (DCL). 35. Measurements between the length of the ventral ligule (VLL) and the length of the ventral cirri (VCL).

*Nereis (Hediste) diversicolor* Hartmann-Schröder 1996: 201–204, fig. 88a–c  
*Hediste diversicolor* Malmgren 1867: 165–166, pl. 28, fig. 28.

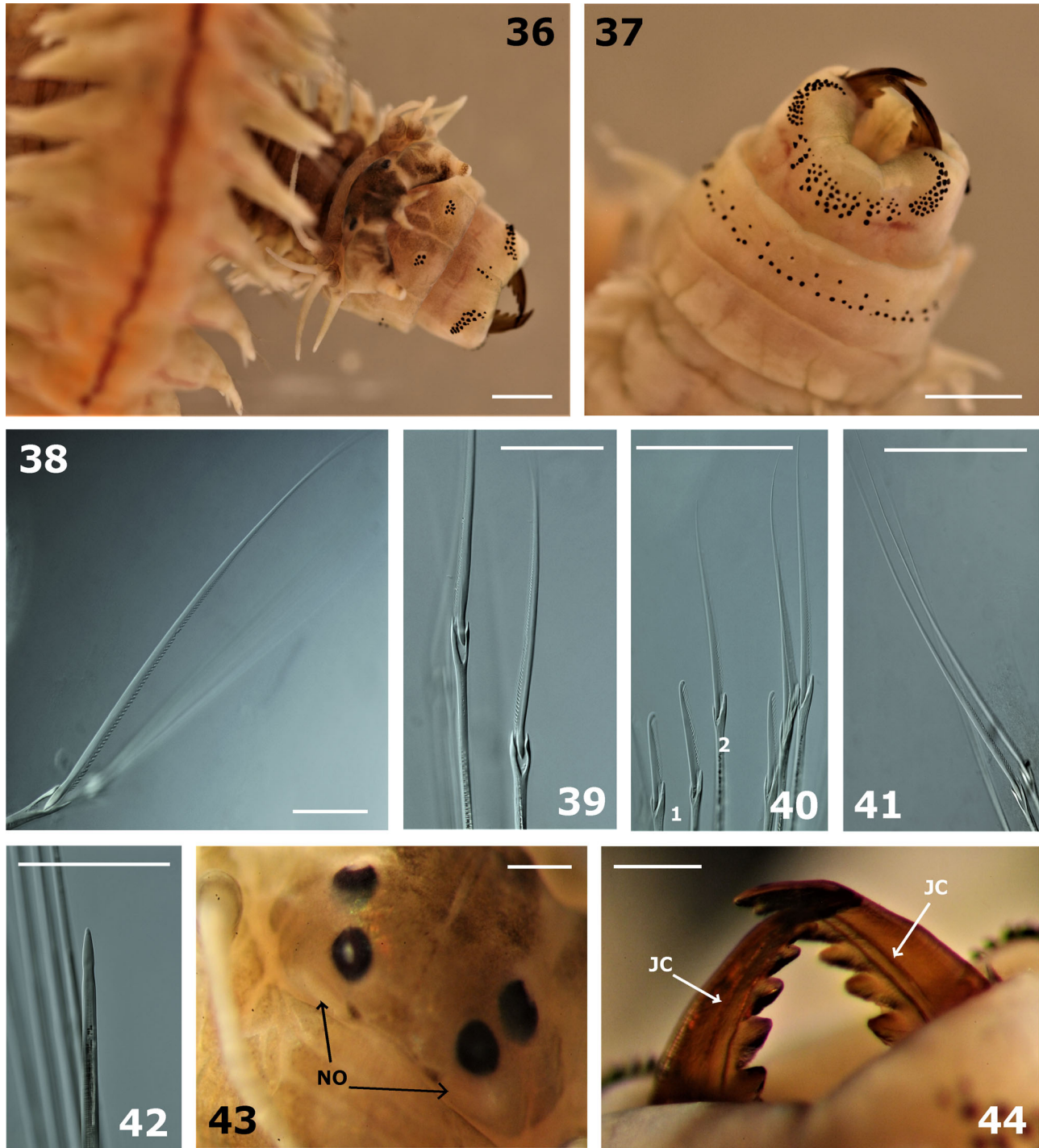
**Type material.** NEOTYPE AND HOLOGENOPHORE: NTNU-VM82082, 1 spm, Norway, Grimstad, 58°17'52.8"N, 8°32'20.4"E, low tide, muddy sand and gravel, collected by Eivind Oug, 14-04-2019. GenBank (COI): OP038792.

**Other material.** DBUA0002458.01.v01-v04 and DBUA0002458.02.v01-v05, 9 spms, Portugal, Sado estuary, 38°29'24.0"N, 8°48'54.0"W, low tide, muddy sand and gravel, collected by Marcos AL Teixeira, Pedro E Vieira, Bruno R Sampieri, Jorge Lobo and Claudia Hollatz, 31-07-2018; DBUA0002457.01.v01-v18, 18 spms, 38°29'52.8"N, 8°50'16.8"W, low tide, muddy sand and gravel, collected by Marcos AL Teixeira, Pedro E Vieira, Bruno R Sampieri, Jorge Lobo and Claudia Hollatz, 28-02-2018. DBUA0002459.01.v01, 1 spm, Portugal, Lima estuary, 41°41.04'N, 8°49.68'W, low tide, muddy sand and gravel, collected by Marcos AL Teixeira, Pedro E Vieira and Bruno R Sampieri; DBUA0002459.02.v01-v02, 2 spms, 41°41.76'N, 8°48.78'W, low tide, muddy sand and gravel, collected by Marcos AL Teixeira, Pedro E Vieira and Bruno R Sampieri; DBUA0002459.03.v01-v20, 20 spms, 41°42.06'N, 8°44.94'W, low tide, muddy sand and gravel, collected by Marcos AL Teixeira, Pedro E Vieira and Bruno R Sampieri. DBUA0002460.01.v01-v20 and DBUA0002460.02.v01-v06, 26 spms, Portugal, Aveiro lagoon, 40°38'02.4"N, 8°40'30.0"W, low tide, muddy sand and gravel, collected by Marcos AL Teixeira, Pedro E Vieira, Bruno R Sampieri and Ascensão Ravara, 28-02-2018. DBUA0002461.01.v01-v20, DBUA0002461.02.v01-v05, 25 spms, Portugal, Minho estuary, 41°52'55.2"N, 8°49'44.4"W, low tide, muddy sand and gravel, collected by Marcos AL Teixeira, 28-02-2018. DBUA0002455.01.v01-v03 and DBUA0002455.02.v01-v02, 5 spms, Spain, Lagares, 42°12'07.2"N, 8°46'40.8"W, low tide, muddy sand and gravel, collected by Marcos AL Teixeira, 23-10-2017. DBUA0002456.01.v01-v09 and MTHD015-20, 10 spms, Spain, Ferrol, 43°29'34.8"N, 8°14'56.4"W, low tide, muddy sand and gravel, collected by Julio Parapar, 26-06-2018. DBUA0002462.01.v01-v10, 10 spms, France, Brest, 48°24'21.6"N, 4°22'01.2"W, low tide, muddy sand and gravel, collected by Juan Pardo, 14-09-2019. NTNU-VM 82080-82081 and NTNU-VM 82083-82084, 4 spms, Norway, Grimstad, 58°17'52.8"N, 8°32'20.4"E,

low tide, muddy sand and gravel, collected by Eivind Oug, 14-04-2019; NTNU-VM 76340–76341, 2 spms, Norway, Trondheim, 63°26'09.6"N, 10°29'56.4"E, low tide, muddy sand and gravel, 04-09-2018.

**Diagnosis.** Body usually with a prominent dorsal blood vessel; medium-sized worm stout anteriorly, posteriorly gradually tapering toward pygidium. Around 50–90 chaetigers. Colour variable between yellow-greenish or yellowish-brown in preserved specimens. Head wider than long; 2.7 times longer than antennae. Palpophore twice as long as the antennae. Distance between the anterior eyes 1.3 times longer than the posterior ones. Postero-dorsal cirri as long as body width or slightly shorter; postero-dorsal cirri reaching chaetiger 4–5. The postero-dorsal cirri can sometimes surpass the body's width and usually doubles the length of the antero-dorsal one; 1.7–2.6 times longer than the antero-dorsal cirri. Antero-dorsal cirri 1.3 times longer than palpophore. Pharynx consisting of maxillary and oral ring with conical paragnaths: Area I with 2–6 paragnaths forming a longitudinal line or a shapeless group. Area II with 9–23 paragnaths (single side) forming a diagonal thick line. Area III in a transverse band of 24–52 paragnaths. Area IV with 19–38 paragnaths (single side) in arched rows, forming a 'C' shape group in the left side; inverted 'C' in the right one. Area V absent. Area VI with 3–8 paragnaths (single side) in small clusters. Area VII–VIII with two bands of paragnaths, the posterior one with twice (20–26) as many paragnaths as the anterior one (10–13). Pair of dark brown jaws, each with 6–8 denticles. Dorsal cirri shorter than dorsal ligule throughout the body; much shorter in median parapodia (three times). Ventral cirri shorter than ventral ligule throughout the body; much shorter in posterior parapodia (three times). Notopodial prechaetal lobe shorter than median ligule throughout the body. Spiniger chaetae more numerous than falcigers throughout the body. Widespread in the NE Atlantic, Norway and Baltic Sea; also present in the NW Atlantic coasts.

**Molecular data.** COI, ITS2 and 28S sequences as in specimens DBUA0002455.01.v01-v03, DBUA0002455.02.v01-v02, DBUA0002456.01.v01-v09, MTHD015-20, DBUA0002457.01.v01-v18, DBUA0002458.01.v01-v04, DBUA0002459.01.v01, DBUA0002459.02.v01-v02, DBUA0002459.03.v01-v20, DBUA0002460.01.v01-v20, DBUA0002461.01.v01-v20, DBUA0002462.01.v01-v10, NTNU-VM 82080-82084 and NTNU-VM 76340-76341 (Supplemental Table S2, dx.doi.org/10.6084/m9.figshare.19224600). Genetic distances are given in Table 4. Phylogenetic relationship as in Fig. 3, belonging to MOTU 2 and characterized by the high intraspecific



**Figs 36–44.** *Hediste diversicolor* s.s. (MOTU 2). 36. Scale bar = 1 mm. Preserved specimen (DBUA0002459.03.v06), with a visible blood vessel and focus on the prostomium and pharynx, dorsal view. 37. Scale bar = 1 mm. Focus on the pharynx, ventral view (DBUA0002459.03.v06). 38. Scale bar = 50.0  $\mu$ m. Neurochaeta, supracicular fascicle: homogomph spiniger with long blades, chaetiger 29 (DBUA0002460.02.v06). 39. Scale bar = 50.0  $\mu$ m. Neurochaeta, supracicular fascicle: homogomph spiniger, chaetiger 10 (NTNU-VM82084). 40. Scale bar = 100  $\mu$ m. Neurochaeta, subacicular fascicle: heterogomph falciger (1), heterogomph spiniger (2), chaetiger 10 (NTNU-VM82084). 41. Scale bar = 100  $\mu$ m. Notochaetae: homogomph spinigers, chaetiger 29 (DBUA0002460.02.v06). 42. Scale bar = 100  $\mu$ m. Neurochaeta, supracicular fascicle: fused falciger, chaetiger 45 (NTNU-VM82084). 43. Scale bar = 0.2 mm. Photo (DBUA0002459.03.v08) of the nuchal organs (NO). 44. Scale bar = 0.2 mm. Jaw picture with two canals (JC) close to the inner edge (DBUA0002459.03.v06).

divergence within some populations that can reach up to 7.5% COI K2P. These distances can be achieved even in specimens from the same estuary (e.g. Minho and Lima estuaries). Interspecific COI mean distances to the closest and distant neighbour are 7.5% (K2P, MOTU 3) and 8.2% (K2P, MOTU 5), respectively. High number of BINs (35, Fig. 3, Table 3) and COI haplotypes (Fig. 5, Table 2) also characterize this MOTU. DOI for the neotype specimen's Barcode Index Number (BIN): [dx.doi.org/10.5883/BOLD:ACF4936](https://dx.doi.org/10.5883/BOLD:ACF4936).

**Distribution and habitat.** North-east Atlantic Ocean, from Norwegian Sea to Morocco; Baltic Sea. Also reported in North America (Einfeldt *et al.*, 2014). In the Baltic Sea and Skagerrak, it occurs in sympatry with *Hediste* sp. B1 and *H. astae* sp. nov. (described below) (Fig. 4). Mostly found in intertidal areas, making burrows in black muddy sand, often under brackish conditions. Commonly used as bait by anglers.

**Reproduction.** Available data on reproduction have been accumulated over time and most likely represent different lineages. Reproduction, including spawns and broods of embryos at 10-week trochophore/demersal nectochaeta stage, occurs at favourable levels of 5–27 salinity. Egg sizes between 200–250  $\mu\text{m}$  were reported for the North Atlantic coastal populations (Bartels-Hardege & Zeeck, 1990; Christensen, 1980; Dales, 1950; Müller, 1776; Scaps, 2002; Smith, 1964).

**Description.** Specimens used: NTNU-VM82084; DBUA0002459.03.v12, DBUA0002460.02.v06, DBUA0002460.02.v05 and Minho samples with everted pharynx for paragnath counts: DBUA0002461.01.v01-v05.

**Body/measurements.** Body with a prominent dorsal blood vessel; stout anteriorly, posteriorly gradually tapering toward pygidium. Colour in preserved specimens yellowish-brown. Neotype, NTNU-VM82084, posteriorly incomplete, total length = 24 mm, L15 = 8.35 mm, W15 = 1.27 mm, and 56 chaetigers. Non-types, DBUA0002459.03.v12, DBUA0002460.02.v06, posteriorly incomplete, TL = 30–33 mm, L15 = 11.52–13.12 mm, W15 = 1.6–1.75 mm, with 51–71 chaetigers. Non-type, DBUA0002460.02.v05, complete, TL = 30 mm, L15 = 13.52 mm, W15 = 1.65 mm, with 71 chaetigers.

**Head.** Prostomium pyriform, 1.5 times wider than long; 2.7 times longer than antennae. Palps with a short round or conical palpostyle (Fig. 36); palpophore slightly longer than wide, shorter than the entire length of

prostomium. Antennae separated, gap half of antennal diameter (Fig. 36); tapered, half the length of the palpophore. Eyes black, anterior and posterior pairs well separated (Fig. 43). Anterior pair of eyes round to oval shaped, wider than antennal diameter; posterior pair of eyes round to oval shaped, subequal to anterior pair. Distance between the anterior eyes 1.3 times longer than the posterior ones (Fig. 33). Nuchal organs deeply embedded, transverse, slightly wider than posterior eyes (Fig. 43).

**Apodous anterior segment and tentacular cirri.** Apodous anterior segment 3 times wider than long, 1.5 times longer and wider than chaetiger 1. Tentacular cirri shorter than or subequal to body width in median segments. Tentacular cirri pattern: postero-dorsal cirri 1.7–2.6 times longer than antero-dorsal ones; postero-dorsal reaching chaetiger 4–5. Antero-dorsal cirri reaching chaetiger 2–3; 1.3 times longer than palpophore. Antero-ventral cirri slightly shorter than postero-ventral ones; antero-ventral shorter than palpophore. Dorsal cirrophores wrinkled, cylindrical; postero-dorsal cirrophores 1.4 times the length of postero-ventral wrinkled ones.

**Pharynx.** Pair of dark brown jaws, each with 6–8 denticles; 2 longitudinal canals emerging from pulp cavity, both closer to the inner edge (Fig. 44). Pharynx consisting of maxillary and oral ring with conical paragnaths (Figs 36–37): Area I with 2–6 paragnaths forming a longitudinal line or a shapeless group; Area II with 9–23 paragnaths (single side) forming a diagonal thick line; Area III in a transverse band of 24–52 paragnaths; Area IV with 19–38 paragnaths (single side) in arched rows, forming a 'C' shape group in the left side, inverted 'C' in the right one; Area V absent; Area VI with 3–8 paragnaths (single side) in small clusters; Area VII–VIII with two bands of paragnaths, the posterior one with twice (20–26) as many paragnaths as the anterior one (10–13).

**Notopodia.** Dorsal cirrus slender, tapering, shorter than dorsal ligule throughout body (Fig. 34), not reaching tip of dorsal ligule; much shorter than ligule in median body, 2 times shorter in anterior (Fig. 13) and posterior parapodia (Fig. 15), 3 times shorter in median parapodia (Fig. 14). Cirrus longer than proximal part of dorsal ligule in anterior parapodia (Fig. 13), subequal in median (Fig. 14) and posterior parapodia (Fig. 15); cirri inserted one-third of the parapodia throughout the body (Figs 13–15). Dorsal ligule subtriangular with tapering tip, subequal to slightly longer than median ligule throughout the body (Figs 13–15). Distal part of dorsal ligule

longer than proximal one in anterior (Fig. 13) and median parapodia (Fig. 14), subequal to proximal in posterior ones (Fig. 15). Notopodial prechaetal lobe shorter than median ligule throughout the body (Figs 13–15).

**Neuropodia.** Neuracicular ligule conical with distinct superior and inferior lobes with similar size; subequal in width to ventral ligule in anterior parapodia (Fig. 13), 1.75 times in median (Fig. 14) and posterior ones (Fig. 15). Neuracicular ligule longer than ventral ligule throughout the body. Ventral ligule conical, 2 times shorter than dorsal ligule in median parapodia (Fig. 14), 1.30 times smaller in anterior (Fig. 13) and posterior ones (Fig. 15). Ventral cirri slender with tapering tip, smaller than ventral ligule throughout body (Fig. 35); 2.3 times shorter than ventral ligule in anterior parapodia (Fig. 13), 1.8 times shorter in median ones (Fig. 14), gradually diminishing in size in posterior ones, around 3.3 times shorter (Fig. 15). Neuropodial postchaetal lobe well developed in anterior parapodia, gradually diminishing in size towards mid-body (well visible at least until chaetiger 32), hardly distinguishable posteriorly.

**Chaetae.** Notochaetae with homogomph spinigers; spinigers with coarsely serrated blade, evenly spaced (Fig. 41), numerous and present throughout the whole body. Neurochaetal supracicular fascicle with homogomph spinigers and heterogomph falcigers, both present throughout the whole body; spinigers similar to notopodial ones (Fig. 38), more numerous than falcigers in same fascicle; falcigers similar to the subacicular ones, replaced with a large fused falciger in the posteriormost chaetigers (Fig. 42), usually in the last 10–15 chaetigers. Neurochaetal subacicular fascicle with heterogomph spinigers (Fig. 40) and heterogomph falcigers (Fig. 40), both present throughout the whole body; spinigers similar to notopodial ones, more numerous than falcigers; falcigers with slender serrated long blade.

**Pygidium.** With pair of cylindrical slender anal cirri, as long as last 6–7 parapodia.

**Remarks.** The taxonomic history of *Hediste diversicolor* is intricate and has been difficult to unravel. Müller (1776) provided a short and vague diagnosis of the species, based on previous records referring to material from Denmark (likely, Copenhagen) and western Norway (Ström, 1762), with no illustrations. Notwithstanding this being considered as the formal original description of the species (Oug et al., 2014), more detailed descriptions and illustrations were given in those previous records (Salazar-Vallejo et al., 2021).

Müller kept a large collection of specimens (Anker, 1950), but no original material is presently known to exist (Oug et al., 2014). Knowing now that *Hediste diversicolor* is a species complex with multiple genetically evolved entities, we find it necessary to select a neotype to provide nomenclatural stability and a physical specimen preserved for later reference. In accordance with our results, we find it reasonable to select a specimen from MOTU 2 (*H. diversicolor* s.s.), collected in the North European Sea (Norway), as neotype.

The specimens of *H. diversicolor* s.s. examined in this study present a higher SIMPER intra-morphometric variation between the analysed proportions when compared with the rest of the complex, similarly to the molecular results regarding the intraspecific COI divergence. *Hediste diversicolor* s.s. have similar proportions to *Hediste* sp. B1, and the morphometric distinction between the two species can only be partially achieved if comparing the antenna length (shorter measurements) against either the similar length of the postero-dorsal cirri, antero-dorsal cirri and head (Figs 33–35, Table 6). Evidence of hybridization between *H. diversicolor* s.s. and *Hediste* sp. B1 is partially seen in the molecular nuclear data and alloenzymes (Audzijonyte et al., 2008), which might not support reproductive isolation in the scope of the more restrictive biological species concept. The other two lineages studied herein, corresponding to *H. astae* sp. nov. and *H. pontii* sp. nov. described below, present smaller and larger morphometric SIMPER proportions, respectively, when comparing with *H. diversicolor* s.s. The most significant distinguishing proportions are the length of the dorsal/ventral ligules, the length/width of the worm, the length/height of the parapodia, the width of the worm with/without parapodia, and both the distance of the posterior eyes and the length of the palps/width of the head (Table 6). *Hediste diversicolor* s.s. is further distinguished from the other two species by the higher number of paragnaths (sometimes twice the amount), especially in Areas III and IV, which may be a diagnostic feature (see Table 5). However, phenotypic variation is high among the specimens. Additionally, the distance between the anterior eyes is clearly greater than the posterior ones, unlike in *H. astae* sp. nov. which has subequal to slightly longer distances (Fig. 33). Furthermore, dorsal cirri appear to be much shorter than dorsal ligule in median parapodia (three times), instead of gradually diminishing in size throughout the body as seen in the other two new species. The proportion between the ventral cirri and ventral ligule is also very variable throughout the body, but appears to be much shorter than ventral ligule in posterior parapodia (three times) (see

**Table 7** for a summary comparison between morphometric measurements based on scatter plots).

For a major review of the biology, ecology and potential use of *Hediste diversicolor* see Scaps (2002). The complete mitochondrial genome from an adult *H. diversicolor* specimen, collected by Andreas Hagemann in Trondheims fjord, Leangbukta, Norway at 63°26'20.9"N, 10°28'28.6"E, was sequenced by Gomes-dos-Santos *et al.* (2021). The specimen is deposited at the Interdisciplinary Center of Marine and Environmental Research – CIIMAR (Prof. Filipe Castro, [filipe.castro@ciimar.up.pt](mailto:filipe.castro@ciimar.up.pt)) under the voucher number 4HDIV3 and GenBank accession number MW377219.

*Hediste pontii* Teixeira, Ravara, Langeneck & Bakken  
sp. nov.

(Figs 16–18, 23, 45–53)

urn:lsid:zoobank.org:act: 84C335DE-6EB8-48B0-9DA3-DD80D40E991D

**Type material.** HOLOTYPE AND HOLOGENOPHORE: 1 spm, DBUA0002465.01.v01, Italy, Venezia Lagoon, 45°20'13.2"N, 12°16'30.0"E, near shore at 0.5–1 m depths, muddy sand and gravel, collected by Massimo Ponti, 10-07-2018, GenBank COI: OPO38876. PARATYPES AND PARAGENOPHORES: DBUA0002465.02.v01-v02 and DBUA0002465.02.v03-v20, 20 spms, 45°20'13.2"N, 12°16'30.0"E, near shore at 0.5–1 m depths, muddy sand and gravel, collected by Massimo Ponti, 10-07-2018.

**Other material.** DBUA0002465.03.v01-v07, Italy, Venezia Lagoon, 7 spms, 45°20'13.2"N, 12°16'30.0"E, near shore at 0.5–1 m depths, muddy sand and gravel, collected by Massimo Ponti, 10-07-2018.

**Diagnosis.** Medium- to large-sized worm stout anteriorly, posteriorly gradually tapering toward pygidium. Around 60–100 chaetigers. Colour yellowish-brown in preserved specimens. Head wider than long; 3 times longer than antennae. Palpophore 2.5 times longer than the antennae. Distance between the anterior eyes 1.3 times longer than the posterior ones. Postero-dorsal cirri clearly shorter than body width in median body (<0.75 ratio); reaching chaetiger 2–3. The postero-dorsal cirri usually doubles the length of the antero-dorsal one; 1.5–2.7 times longer than the antero-dorsal cirri. Antero dorsal cirri 1–1.4 times longer than palpophore. Pharynx consisting of maxillary and oral ring with conical paragnaths: Area I with 1–3 paragnaths forming a longitudinal line or a shapeless group. Area II with 10–17 paragnaths (single side) forming a diagonal

thick line. Area III in a transverse band of 22–25 paragnaths. Area IV with 17–20 paragnaths (single side) in arched rows, forming a 'C' shape group in the left side; inverted 'C' in the right one. Area V absent. Area VI with 3–8 paragnaths (single side) in small clusters. Area VII–VIII with two bands of paragnaths, the posterior one with twice (20–24) as many paragnaths as the anterior one (10–12). Pair of dark brown jaws, each with 9–10 denticles. Dorsal cirri shorter than dorsal ligule, gradually diminishing in size throughout the body. Ventral cirri shorter than ventral ligule throughout the body; much shorter in anterior and median parapodia (2.6 times). Notopodial prechaetal lobe longer than median ligule in posterior parapodia. Spiniger chaetae more numerous than falcigers throughout the body. Geographic distribution limited to the Adriatic Sea.

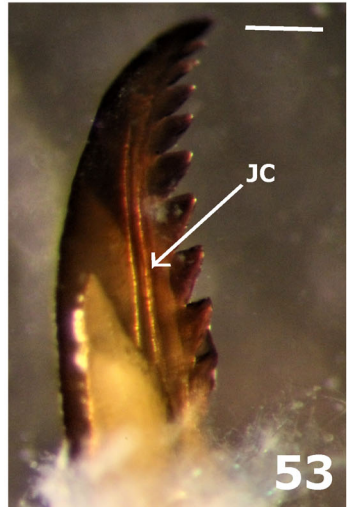
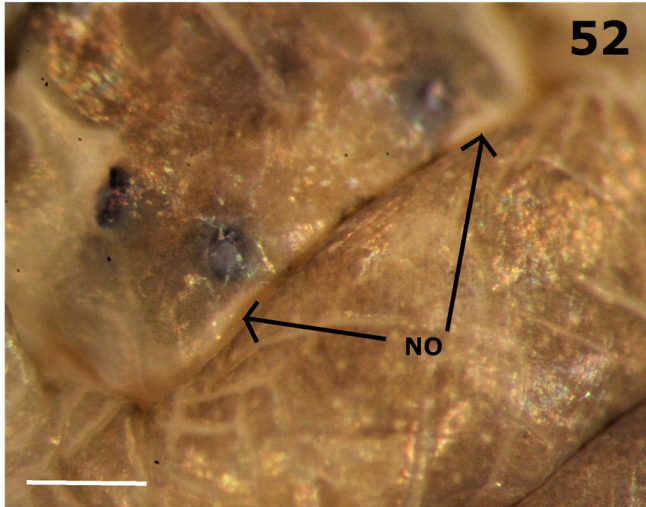
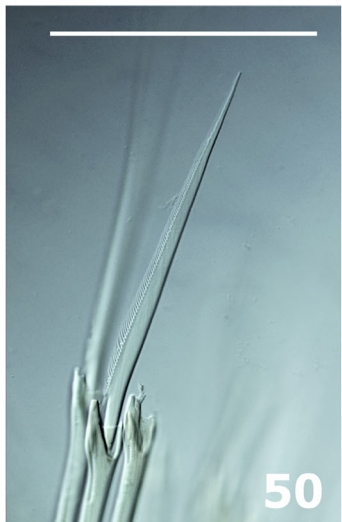
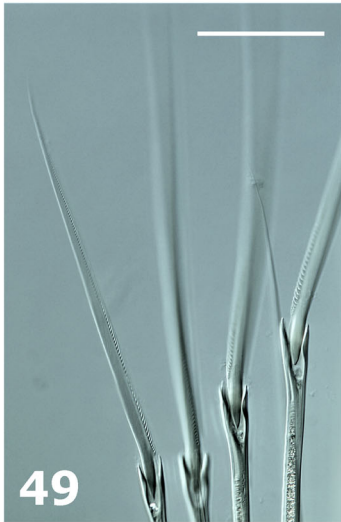
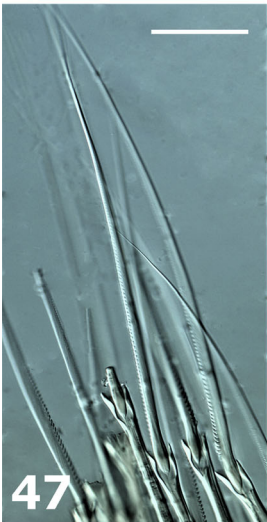
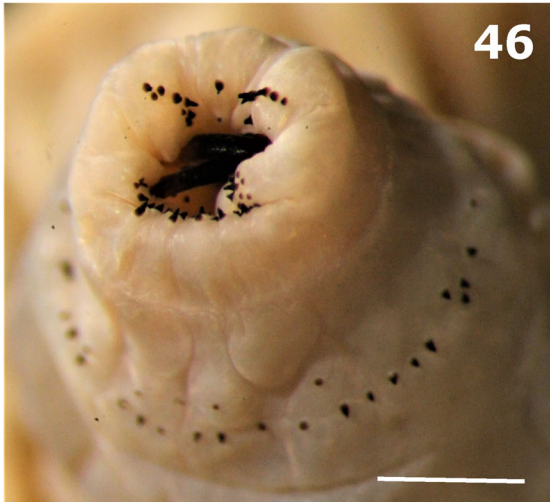
**Molecular data.** COI, ITS2 and 28S sequences as in specimens DBUA0002465.01.v01 and DBUA0002465.02.v01-v20 (**Supplemental Table S2**). COI haplotype information and genetic distances as in **Tables 2** and **4**, respectively. Phylogenetic relationships as in **Fig. 3**, belonging to MOTU 3, with high support values and low intraspecific (<3%) genetic divergence for both the mitochondrial and nuclear markers. Interspecific COI mean distances to the closest and distant neighbour are 4.4% (K2P, MOTU 4) and 7.5% (K2P, MOTU 2) respectively. DOI for the species' Barcode Index Number (BIN): [dx.doi.org/10.5883/BOLD:ADW0792](https://dx.doi.org/10.5883/BOLD:ADW0792).

**Etymology.** The new species is named after Massimo Ponti to recognize his great kindness in collecting a large number of *Hediste* specimens from the Adriatic Sea on the behalf of the authors of this paper.

**Distribution and habitat.** Mediterranean, restricted to the Adriatic Sea (**Fig. 4**). Intertidal, making burrows in black muddy sand, usually under high salinity waters. Commonly used as bait by anglers.

**Description.** Specimens used: DBUA0002465.01.v01, DBUA0002465.02.v03 and DBUA0002465.02.v12. Specimens used only for chaetae observations: DBUA0002465.02.v01-v02. Specimens used only for paragnath counts: DBUA0002465.02.v04-v05.

**Body/measurements.** Body stout anteriorly, posteriorly gradually tapering toward pygidium. Colour in preserved specimens yellowish-brown. Holotype, DBUA0002465.01.v01, complete, total length = 62 mm, L15 = 15.2 mm, W15 = 2.8 mm, and 74 chaetigers. Paratypes, DBUA0002465.02.v03 and DBUA0002465.



02.v12, posteriorly incomplete, TL = 50–87 mm, L15 = 16.8–17.6 mm, W15 = 2.6–3.2 mm, with 62–95 chaetigers.

**Head.** Prostomium pyriform (Fig. 45), 1.3–1.4 times wider than long; 3.2 times longer than antennae. Palps with a short round palpostyle (Fig. 23); palpophore slightly longer than wide, shorter than the entire length of prostomium. Antennae separated, gap half of antennal diameter (Fig. 45); tapered, 2–2.5 times shorter than the palpophore. Eyes black, anterior and posterior pairs well separated (Fig. 52). Anterior pair of eyes round to oval shaped, wider than antennal diameter; posterior pair of eyes round to oval shaped, subequal to anterior pair. Distance between the anterior eyes, 1.3 times longer than the posterior ones (Fig. 33). Nuchal organs deeply embedded, transverse, twice as wider as posterior eyes (Fig. 52).

**Apodous anterior segment and tentacular cirri.**

Apodous anterior segment 2.5 times wider than long, 1.5 times longer and slightly wider than chaetiger 1. Tentacular cirri considerably shorter than body width in median segments. Tentacular cirri pattern: postero-dorsal cirri 1.5–2.7 times longer than antero-dorsal ones; postero-dorsal reaching chaetiger 2–3. Antero-dorsal cirri reaching chaetiger 1–2; 1.4 times longer than palpophore. Antero-ventral cirri slightly shorter than postero-ventral ones; antero-ventral subequal to slightly longer than palpophore. Dorsal cirrophores wrinkled, cylindrical; postero-dorsal cirrophores long, 2 times the length of postero-ventral wrinkled ones.

**Pharynx.** Pair of dark brown jaws, each with 9–10 denticles; 2 longitudinal canals emerging from pulp cavity, both closer to the inner edge (Fig. 53). Pharynx consisting of maxillary and oral ring with conical paragnaths (Figs 45, 46): Area I with 1–3 paragnaths forming a longitudinal line or a shapeless group; Area II (single side) with 10–17 paragnaths forming a diagonal thick line; Area III in a transverse band of 22–25 paragnaths; Area IV (single side) with 17–20 paragnaths in arched rows, forming a ‘C’ shape group in the left side, inverted ‘C’

in the right one; Area V absent; Area VI (single side) with 3–8 conical paragnaths in small clusters; Area VII–VIII with two bands of paragnaths, the posterior one with twice (20–24) as many paragnaths as the anterior one (10–12).

**Notopodia.** Dorsal cirrus slender, tapering, shorter than dorsal ligule throughout body (Fig. 34), not reaching tip of dorsal ligule, gradually diminishing in size throughout the body; 2.4 times shorter in anterior parapodia (Fig. 16), 2.9 times in median (Fig. 17) and 3 times in posterior ones (Fig. 18). Cirrus slightly longer than the length of proximal part of dorsal ligule throughout the body; cirri inserted one-third of the parapodia throughout the body (Figs 16–18). Dorsal ligule subtriangular with tapering tip, longer than median ligule throughout the body, much longer in posteriormost chaetigers (Fig. 18). Distal part of dorsal ligule longer than proximal one throughout the body. Notopodial prechaetal lobe shorter than median ligule in anterior (Fig. 16) and median parapodia (Fig. 17), longer in posterior ones (Fig. 18).

**Neuropodia.** Neuracicular ligule conical with distinct superior and inferior lobes with similar size; 1.6 times the width of ventral ligule in anterior (Fig. 16) and posterior parapodia (Fig. 18), 1.9 times in median ones (Fig. 17). Neuracicular ligule subequal in length to ventral ligule in anterior (Fig. 16) and median parapodia (Fig. 17), 1.3 times longer in posterior ones (Fig. 18). Ventral ligule conical, 1.7 times shorter than dorsal ligule in anterior parapodia (Fig. 16), 2 times shorter in median (Fig. 17) and posterior ones (Fig. 18). Ventral cirri slender with tapering tip, smaller than ventral ligule throughout body (Fig. 35); 2.6 times shorter than ventral ligule in anterior (Fig. 16) and median parapodia (Fig. 17), 2 times shorter in posterior ones (Fig. 18). Neuropodial postchaetal lobe well developed in anterior parapodia, gradually diminishing in size towards mid-body (well visible at least until chaetiger 27), hardly distinguishable posteriorly.

**Figs 45–53.** *Hediste pontii* sp. nov. (MOTU 3). 45. Scale bar = 1 mm. Preserved specimen (DBUA0002465.02.v04), with focus on the prostomium and pharynx, dorsal view. 46. Scale bar = 1 mm. Focus on the pharynx, ventral view (DBUA0002465.02.v04). 47. Scale bar = 50.0 µm. Neurochaeta, supracicular fascicle: homogomph spiniger with long blades, chaetiger 31 (DBUA0002465.02.v02). 48. Scale bar = 50.0 µm. Neurochaeta, supracicular fascicle: fused falciger (1), chaetiger 62 (DBUA0002465.02.v02). 49. Scale bar = 50.0 µm. Notochaetae: homogomph spinigers, chaetiger 10 (DBUA0002465.02.v01). 50. Scale bar = 100 µm. Neurochaeta, subacicular fascicle: heterogomph spinigers, chaetiger 10 (DBUA0002465.02.v01). 51. Scale bar = 50.0 µm. Neurochaeta, subacicular fascicle: heterogomph falcigers, chaetiger 10 (DBUA0002465.02.v02). 52. Scale bar = 0.4 mm. Photo (DBUA0002465.02.v05) of the nuchal organs (NO). 53. Scale bar = 0.2 mm. Jaw picture with two canals (JC) close to the inner edge (DBUA0002465.02.v05).

**Chaetae.** Notochaetae with homogomph spinigers; spinigers with coarsely serrated blade, evenly spaced (Fig. 49), numerous and present throughout the whole body. Neurochaetal supracircular fascicle with homogomph spinigers (Fig. 47) and heterogomph falcigers, both present throughout the whole body; spinigers similar to notopodial ones, more numerous than falcigers in same fascicle; falcigers similar to subacicular ones, replaced with a large fused falciger in the posteriormost chaetigers (Fig. 48), usually in the last 10–15 chaetigers. Neurochaetal subacicular fascicle with heterogomph spinigers (Fig. 50) and heterogomph falcigers (Fig. 51), both present throughout the whole body; spinigers similar to notopodial ones, slightly more numerous than falcigers; falcigers with slender serrated long blade.

**Pygidium.** Not observed. Broken.

**Remarks.** *Hediste pontii* sp. nov. is a member of the European *Hediste diversicolor* species complex, thus morphologically highly similar to *H. diversicolor* s.s. and the remaining species of the complex. However, some variations in the size of specific morphological characters can be found. Specimens from this species usually present a higher number of chaetigers, wider and longer body, and overall larger morphometric proportions compared with the remaining species of the complex. General PCA and SIMPER data show considerable morphometric differences, with the most significant proportions being the length of the dorsal/ventral ligules of median segments, the length/height of the parapodia of median segments, the worm's length/width, and the length of the palps/antero-dorsal cirri (Table 6). Proportions for the length of the antennae and head are larger for *H. pontii* sp. nov. than for *H. diversicolor* s.s. and *H. astae* sp. nov. (described below). However, the morphometric proportions used to distinguish *H. pontii* sp. nov. from *H. diversicolor* s.s. and *H. astae* sp. nov., usually have the same values as for *Hediste* sp. B1 (MOTU 1) and mostly cannot be used to separate the latter from *H. pontii* sp. nov. Nevertheless, despite a considerably longer head size and palps, antennae length has similar morphometric measurements as *Hediste* sp. B1. Furthermore, *H. pontii* sp. nov. has larger proportions between the length of the head when compared with the distance between the posterior and anterior eyes of *Hediste* sp. B1 (Table 6).

The distance between the anterior eyes is clearly greater than the posterior ones, unlike in *H. astae* sp. nov. which has subequal to slightly longer distances. Besides geographic distribution, the new species unique to the Adriatic Sea is further distinguished from *H. astae* sp. nov. by the ratio between the number of

spiniger and falciger chaetae in the neuropodial subacicular fascicle, where spinigers are more numerous than falcigers throughout the body. However, *H. pontii* sp. nov. shares with the latter species a similar proportion pattern between the length of the dorsal cirri against the dorsal ligule, where the dorsal cirri gradually diminish in size throughout the body, unlike in *H. diversicolor* s.s. where it seems to be much shorter in median parapodia. The proportion between the ventral cirri and ventral ligule may be a diagnostic feature since it appears that the ventral cirri is much shorter in both anterior and median parapodia (2.6×), while it is much shorter only in the anterior parapodia (3 times) in *H. diversicolor* s.s. and much shorter in median and posterior parapodia (2 times) in *H. astae* sp. nov. Further distinction between the new species against *H. diversicolor* s.s. and *H. astae* sp. nov. relates to the size of the tentacular cirri that is clearly shorter in *H. pontii* sp. nov., with the postero-dorsal cirri usually only reaching around 0.75 times the body width in median segments (see Table 7). This is further highlighted if we take in consideration that all the analysed specimens from *H. pontii* sp. nov. were clearly larger than the ones from *H. diversicolor* s.s. or *H. astae* sp. nov. yet both the length of the postero-dorsal and antero-dorsal cirri were similar to the analysed specimens from *H. diversicolor* s.s. A lower number of paragnaths (sometimes down to half), especially in Areas III and IV, further distinguishes *H. pontii* sp. nov. from *H. diversicolor* s.s., although there is a high phenotypic variation within the latter species preventing this feature from being 100% accurate (see Table 5).

Very low intraspecific COI variation and clear MOTU delineation also separate this species from the remaining species described from the complex. It is possible that *Hediste* populations from Greece in the Amvrakikos lagoon (Ionian Sea, *Hediste* sp. B3) might belong to this species based on nuclear haplotypes, however more than 4% divergence is present in the COI loci. There is the possibility that unsampled haplotypes occur in the area between Venice and Amvrakikos Lagoon, that hosts several potentially suitable habitats for this species. Thus, eastern Ionian Sea and Northern Adriatic Sea haplotypes might well be two extremes of a continuum of unsampled populations. No morphometric or reproduction data are yet available to confirm the status between Adriatic and Ionian populations.

*Hediste astae* Teixeira, Ravara, Langeneck and Bakken  
sp. nov.

(Figs 19–21, 24, 54–61)

urn:lsid:zoobank.org:act: 0F40A03E-83F1-4510-B6C8-6AD03A260237

**Type material.** HOLOTYPE AND HOLOGENOPHORE: DBUA0002466.03.v01, 1 spm, Greece, Nestos Lagoon, 40°54'36.0"N, 24°52'22.8"E, near shore at 0.5–1 m depths, muddy sand and gravel, collected by Sarah Faulwetter, 28-05-2018, GenBank COI: OP038740. PARATYPES AND PARAGENOPHORES: DBUA0002466.04.v01-v03 and DBUA0002466.04.v04-v07, 7 spms, 40°54'36.0"N, 24°52'22.8"E, near shore at 0.5–1 m depths, muddy sand and gravel, collected by Sarah Faulwetter, 28-05-2018.

**Other material.** DBUA0002466.01.v01-v05, 5 spms, Greece, Evros Lagoon, 40°44'38.4"N, 26°02'13.2"E, near shore at 0.5–1 m depths, muddy sand and gravel, 25-05-2018. DBUA0002466.05.v01-v04, 4 spms, Greece, Ptelea Lagoon, 40°56'13.2"N, 25°14'49.2"E, near shore at 0.5–1 m depths, muddy sand and gravel, collected by Sarah Faulwetter, 26-05-2018. DBUA0002466.02.v01-v06, 6 spms, Greece, Alyki lagoon, 40°57'00.0"N, 25°12'50.4"E, near shore at 0.5–1 m depths, muddy sand and gravel, collected by Sarah Faulwetter, 26-05-2018. DBUA0002466.06.v01-v04, 4 spms, Greece, Axios Lagoon, 40°30'28.8"N, 22°43'40.8"E, near shore at 0.5–1 m depths, muddy sand and gravel, collected by Sarah Faulwetter, 21-05-2018; DBUA0002466.07.v01-v13 and DBUA0002466.08.v01-v12, 25 spms, 40°44'38.4"N, 26°02'13.2"E, near shore at 0.5–1 m depths, muddy sand and gravel, collected by Sarah Faulwetter, 25-05-2018.

**Diagnosis.** Small- to medium-sized worm stout anteriorly, posteriorly gradually tapering toward pygidium. Around 40–90 chaetigers. Colour variable between yellowish-brown or orange-brown in preserved specimens. Head wider than long; 2.5 times longer than antennae. Palpophore twice as long as the antennae. Distance between the anterior eyes subequal to slightly longer to the posterior ones. Most tentacular cirri as long as body width or longer; postero-dorsal cirri reaching chaetiger 4–6. The postero-dorsal cirri usually doubles the length of the antero-dorsal one; 1.4–2 times longer than the antero-dorsal cirri. Antero dorsal cirri 1.7–2 times longer than palpophore. Pharynx consisting of maxillary and oral ring with conical paragnaths: Area I with 1–2 paragnaths forming a longitudinal line or a shapeless group. Area II with 5–15 paragnaths forming a diagonal thick line. Area III in a transverse band of 19–29 paragnaths. Area IV with 13–22 paragnaths in arched rows, forming a 'C' shape group in the left side; inverted 'C' in the right one. Area V absent. Area VI with 3–8 conical paragnaths in small clusters. Area VII–VIII with two tight bands with 11–15 paragnaths each. Pair of dark brown jaws, each with 7–8

denticles. Dorsal cirri shorter than dorsal ligule, gradually diminishing in size throughout the body. Ventral cirri shorter than ventral ligule throughout the body; much shorter in median and posterior parapodia (2 times). Notopodial prechaetal lobe subequal in length to median ligule in anterior and posterior parapodia; shorter in median ones. Falciger chaetae more numerous than spinigers in the neuropodial subacicular fascicle from the anterior and median parapodia.

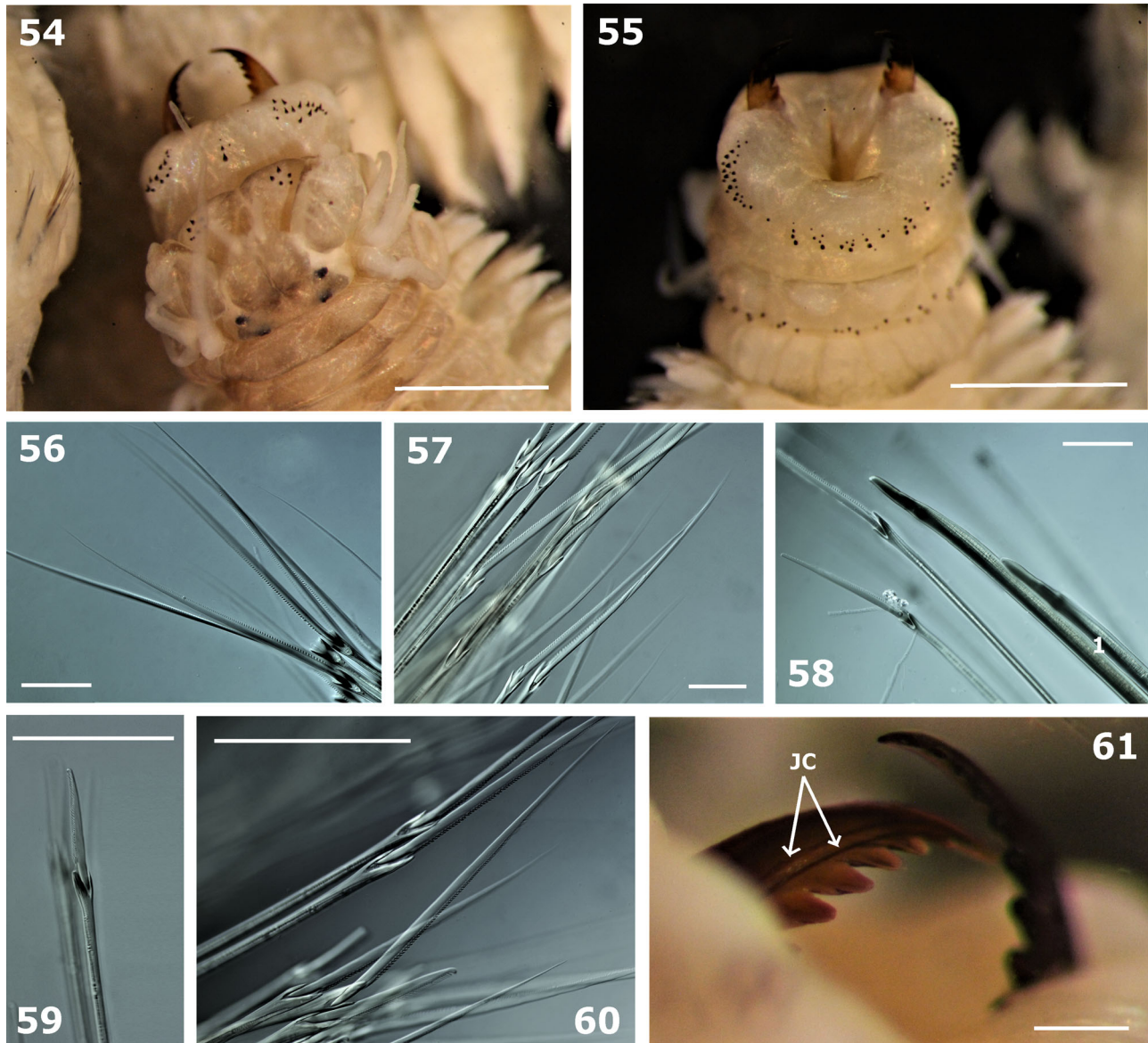
**Molecular data.** COI, ITS2 and 28S sequences as in specimens DBUA0002466.01.v01-v05, DBUA0002466.02.v01-v06, DBUA0002466.03.v01, DBUA0002466.04.v01-v07, DBUA0002466.05.v01-v04, DBUA0002466.06.v01-v04 ([Supplemental Table S2](#)). COI haplotype information and genetic distances as in [Tables 2](#) and [4](#), respectively. Phylogenetic relationship as in [Fig. 3](#), belonging to MOTU 5, with high support values and low intraspecific (COI <3.5%, usually in the higher end of the spectrum) genetic divergence for both the mitochondrial and nuclear markers. Interspecific COI mean distances to the closest and distant neighbour are 7.0% (K2P, MOTU 1) and 8.2% (K2P, *H. diversicolor* s.s.), respectively. DOI for the haplotype's Barcode Index Number (BIN): [dx.doi.org/10.5883/BOLD:AAC7124](https://dx.doi.org/10.5883/BOLD:AAC7124).

**Etymology.** The new species is named after Asta Audzijonyte to recognize her earlier contribution in the detection and separation between 'Species A' and 'B' from the European *Hediste diversicolor* complex.

**Distribution and habitat.** Mediterranean, restricted to the Aegean Sea (Greece). Also present in the Black and Caspian Seas. In the Baltic Sea it occurs in sympatry with *Hediste diversicolor* s.s. and *Hediste* sp. B1 ([Fig. 4](#)). Intertidal, making burrows in black muddy sand, usually under high salinity waters. Commonly used as bait by anglers.

**Description.** Specimens used: DBUA0002466.03.v01, DBUA0002466.08.v04, DBUA0002466.08.v07, DBUA0002466.08.v12, DBUA0002466.02.v05. Specimens used only for chaetae observations: DBUA0002466.04.v02. Specimens used only for paragnath counts: DBUA0002466.02.v04-v06, DBUA0002466.04.v03-v04.

**Body/measurements.** Body stout anteriorly, posteriorly gradually tapering toward pygidium. Colour variable in preserved specimens, yellowish-brown and orange-brown. Holotype, DBUA0002466.03.v01, posteriorly incomplete, total length = 16.4 mm, L15 = 5.6 mm,



**Figs 54–61.** *Hediste astae* sp. nov. (MOTU 3). 54. Scale bar = 1 mm. Preserved specimen (DBUA0002466.02.v04), with focus on the prostomium and pharynx, dorsal view. 55. Scale bar = 1 mm. Focus on the pharynx, ventral view (DBUA0002466.02.v06). 56. Scale bar = 50.0  $\mu$ m. Neurochaeta, supracicular fascicle: homogomph spiniger with long blades, chaetiger 31 (DBUA0002466.04.v02). 57. Scale bar = 50.0  $\mu$ m. Notochaetae: homogomph spinigers, chaetiger 59 (DBUA0002466.02.v05). 58. Scale bar = 50.0  $\mu$ m. Neurochaeta, supracicular fascicle: fused falcigers (1), chaetiger 70 (DBUA0002466.04.v02). 59. Scale bar = 100  $\mu$ m. Neurochaeta, subacicular fascicle: heterogomph falcigers, chaetiger 30 (DBUA0002466.02.v05). 60. Scale bar = 100  $\mu$ m. Neurochaeta, subacicular fascicle: heterogomph spinigers, chaetiger 10 (DBUA0002466.02.v05). 61. Scale bar = 0.2 mm. Jaw picture with two canals (JC) close to the inner edge (DBUA0002466.01.v03).

W15 = 1.5 mm, and 42 chaetigers. Non-types, DBUA0002466.08.v07, DBUA0002466.08.v12, DBUA0002466.02.v05, posteriorly incomplete, TL = 12 – 84 mm, L15 = 5.55 – 18.2 mm, W15 = 1 – 3.9 mm, with 45 – 90 chaetigers. Non type, DBUA0002466.08.v04, complete, total length = 13.3 mm, L15 = 4.775 mm, W15 = 0.76 mm, and 65 chaetigers.

**Head.** Prostomium pyriform (Fig. 54), slightly wider than long; 2.7 times longer than antennae. Palps with a short round palpostyle (Fig. 54); palpophore slightly longer than wide, shorter than the entire length of prostomium. Antennae separated, gap half of antennal diameter (Fig. 54); tapered, half the length of the palpophore. Eyes black, anterior and posterior pairs well separated (Fig. 54). Anterior pair of eyes round to oval shaped,

subequal to antennal diameter; posterior pair of eyes round to oval shaped, subequal to anterior pair. Distance between the anterior eyes, subequal to slightly longer than the posterior ones (Figs 24, 33). Nuchal organs covered, not observed.

**Apodous anterior segment and tentacular cirri.**

Apodous anterior segment 3 times wider than long, 1.5 times longer and wider than chaetiger 1. Tentacular cirri pattern: postero-dorsal cirri 1.7–2 times longer than antero-dorsal ones; postero-dorsal reaching chaetiger 4–6, 1.4 times longer than body width in median segments. Antero-dorsal cirri reaching chaetiger 2–4; 1.7–2 times longer than palpophore. Antero-ventral cirri slightly shorter than postero-ventral ones; antero-ventral shorter subequal in length to the palpophore. Dorsal cirrophores wrinkled, cylindrical; postero-dorsal cirrophores slightly longer, 1.3 times the length of postero-ventral wrinkled ones.

**Pharynx.** Pair of dark brown jaws, each with 9–10 denticles; 2 longitudinal canals emerging from pulp cavity, both closer to the inner edge (Fig. 61). Pharynx consisting of maxillary and oral ring with conical paragnaths (Fig. 54–55): Area I with 1–2 paragnaths forming a longitudinal line or a shapeless group; Area II (single side) with 5–15 paragnaths forming a diagonal thick line; Area III in a transverse band of 19–29 paragnaths; Area IV (single side) with 13–22 paragnaths in arched rows, forming a ‘C’ shape group in the left side, inverted ‘C’ in the right one; Area V absent; Area VI (single side) with 3–8 conical paragnaths in small clusters; Area VII–VIII two tight bands of paragnaths of 11–15 paragnaths each.

**Notopodia.** Dorsal cirrus slender, tapering, shorter than dorsal ligule throughout body (Fig. 34), not reaching tip of dorsal ligule, gradually diminishing in size throughout the body; 2 times shorter in anterior (Fig. 19) and median parapodia (Fig. 20), 2.6 times in posterior ones (Fig. 21). Cirrus shorter than the length of proximal part of dorsal ligule throughout the body; cirri inserted one-half of the parapodia throughout the body (Figs 19–21). Dorsal ligule subtriangular with tapering tip, longer than median ligule throughout the body, much longer in anterior parapodia (Fig. 19). Distal part of dorsal ligule subequal in length to proximal one throughout the body (Figs 19–21). Notopodial prechaetal lobe subequal in length to median ligule in anterior (Fig. 19) and posterior parapodia (Fig. 21), shorter in median ones (Fig. 20).

**Neuropodia.** Neuracicular ligule conical with distinct superior and inferior lobes with similar size, more prevalent in anterior parapodia; 1.2 times the width of ventral

ligule in anterior parapodia (Fig. 19), 2.7 times in median (Fig. 20), 1.8 times in posterior ones (Fig. 21). Neuracicular ligule subequal in length to ventral ligule in anterior parapodia (Fig. 19), 2 times longer in median (Fig. 20), 1.7 times in posterior ones (Fig. 21). Ventral ligule conical, 2 times shorter than dorsal ligule throughout the body (Figs. 19–21). Ventral cirri slender with tapering tip, smaller than ventral ligule throughout body (Fig. 35); 1.2 times shorter than ventral ligule in anterior parapodia (Fig. 19), 2 times shorter in median (Fig. 20) and posterior ones (Fig. 21). Neuropodial postchaetal lobe well developed in anterior parapodia, gradually diminishing in size towards mid-body (well visible at least until chaetiger 20), hardly distinguishable posteriorly.

**Chaetae.** Notochaetae with homogomph spinigers; spinigers with coarsely serrated blade, evenly spaced (Fig. 57), numerous and present throughout the whole body. Neurochaetal supracicular fascicle with homogomph spinigers (Fig. 56) and heterogomph falcigers, both present throughout the whole body; spinigers similar to notopodial ones, more numerous than falcigers in same fascicle; falcigers similar to subacicular heterogomph ones, replaced with a large fused falciger in the posteriormost chaetigers (Fig. 58), usually in the last 10–15 chaetigers. Neurochaetal subacicular fascicle with heterogomph spinigers (Fig. 60) and heterogomph falcigers, both present throughout the whole body; spinigers similar to notopodial ones, less numerous than falcigers in the anterior and median parapodia, more numerous than falcigers in posterior parapodia; falcigers with slender serrated long blade (Fig. 59).

**Pygidium.** With pair of cylindrical slender anal cirri, as long as last 7–8 parapodia.

**Remarks.** *Hediste astae* sp. nov. is a member of the European *Hediste diversicolor* species complex, thus morphologically highly similar to *H. diversicolor* s.s., *Hediste* sp. B1, *Hediste* sp. B3 and *H. pontii* sp. nov. Specimens from this species usually present a low number of chaetigers and have a smaller body, when comparing with the other species of the complex. Though, we found very few specimens, not used in the morphometric analysis, that were very large, reaching 84 mm in length, 4.369 mm in width and 90 chaetigers (e.g. specimen DBUA0002466.02.v05). General PCA and SIMPER data shows considerable morphometric differences, compared with the other species of the complex, and usually smaller proportions. The most significant distinguishing proportions are the width of the worm with/without parapodia, both the distance between the posterior eyes and length of the palps with the width of

the head, both the length of the antennae and palps with the length of the antero-dorsal cirri, and the length of the postero-dorsal cirri/antero-dorsal cirri (Table 6).

Besides being restricted to the Aegean, Caspian and Black Seas, *Hediste astae* sp. nov. is sympatrically distributed in the Baltic Sea together with both *H. diversicolor* s.s. and *Hediste* sp. B1. Some morphological features can, however, distinguish the new species from *H. diversicolor* s.s. The distance between the anterior eyes is subequal to slightly longer to the posterior ones (Fig. 33), unlike in *H. diversicolor* s.s. and *H. pontii* sp. nov. which clearly has greater distances in the anterior eyes. Additionally, *H. astae* sp. nov. has the presence of higher number of falciger chaetae compared with spinigers in the neuropodial subacicular fascicle, usually in the anterior and median parapodia. Furthermore, both *H. astae* sp. nov. and *H. pontii* sp. nov., share a similar proportion pattern between the length of the dorsal cirri against the dorsal ligule, where the dorsal cirri gradually diminish in size throughout the body, unlike in *H. diversicolor* s.s. where it seems to be much shorter in median parapodia. The proportion between the ventral cirri and ventral ligule may be a diagnostic feature since it appears that the ventral cirri is much shorter in both median and posterior parapodia (2 times), while it is much shorter only in the anterior parapodia (3 times) in *H. diversicolor* s.s. and much shorter in anterior and median parapodia (2.6 times) in *H. pontii* sp. nov. Further distinction between the new species against *H. diversicolor* s.s., but especially against *H. pontii* sp. nov., relates to the size of the tentacular cirri that is clearly shorter in *H. pontii* sp. nov., with the postero-dorsal cirri usually only reaching around 0.75 times the body width in median segments, and about the same body width in *H. diversicolor* s.s. However, in *H. astae* sp. nov. the postero-dorsal cirri can sometimes reach up to 1.4 times the width of the body in median segments (see Table 7). A lower number of paragnaths (sometimes down to half), especially in Areas III and IV, further distinguishes *H. astae* sp. nov. from *H. diversicolor* s.s., and may be a diagnostic feature, although phenotypic variation is high among the specimens (see Table 5). Low intraspecific COI variation (although it may reach values slightly higher than 3%, when using Baltic samples) and clear MOTU delineation also separates this species from the remaining described ones from the complex.

## Discussion

As observed by Virgilio et al. (2009), and confirmed in this study, the phylogeographic structure of the European *Hediste diversicolor* comprises at least three

deeply divergent allopatric lineages. Excluding the Baltic Sea, where sympatry seems to occur between three different MOTUs (1, 2 and 5), these allopatric lineages include populations from the NE Atlantic and part of the western Mediterranean Sea (MOTU 2, *H. diversicolor* s.s.); from the Tyrrhenian Sea (MOTU 1, *Hediste* sp. B1); and lastly from the Caspian and Black Seas with the addition of our populations from the northern Aegean Sea (MOTU 5, *H. astae* sp. nov.). In this study, integrative taxonomy supports the addition of a fourth divergent lineage in the Adriatic Sea (MOTU 3, *H. pontii* sp. nov.) as well. *Hediste pontii* sp. nov. displayed an independent morphometric cluster in the PCA (Fig. 22) with a mean inter-cluster variation of 64.80% (SIMPER), which is far higher than those observed in similar polychaete studies (Martin et al., 2017; Teixeira et al., 2020). Molecular evidence for a possible fifth lineage unique to the Ionian Sea (MOTU 4, *Hediste* sp. B3) was also observed, but additional specimens are needed to complement this information with morphological data. The molecular distances between *H. pontii* sp. nov. and *Hediste* sp. B3 are relatively low (4.4% mean COI divergence, Table 4). However, instances of low or even non-existent COI divergence can also be found in other *Hediste* species, e.g. between *H. diadroma* Sato & Nakashima, 2003 and ‘form B’ of *H. atoka* Sato & Nakashima, 2003, both endemic to south of Japan. These sympatric taxa cannot be discriminated using only the COI gene (Tosuji et al., 2019), and the morphology is almost indistinguishable in sexually immature worms (atokes). Yet, their differentiation is still possible but only through the presence of a unique epitokous metamorphosis and different egg size in *H. diadroma* (Table 5; Sato & Nakashima, 2003).

The occurrence of different European lineages can possibly be explained by vicariance events, either caused by the emergence of land barriers, by isolation within glacial refugia or by changes in oceanic currents. These events are known to have triggered allopatric divergence, genetic isolation and speciation in several marine organisms in the region (Patarnello et al., 2007; Wares & Cunningham, 2001; Xavier & Van Soest, 2012). Additionally, divergent selection related to environmental features can lead to genetic differentiation among lineages, promoting local adaptation (Peijnenburg et al., 2004). For example, evidence of different salinity preferences was found between ‘Species A’ and ‘Species B’ of *H. diversicolor*, that could affect their success in competition for habitat in the Baltic regions, despite both being euryhaline (Audzijonyte et al., 2008). The lack of a true pelagic phase can also facilitate a rapid increase of genetic differentiation

between populations (Breton *et al.*, 2003; Virgilio & Abbiati, 2006).

### Sympatry and possible hybridization in the Baltic Sea

The three sympatric lineages found in the Baltic Sea (*Hediste* sp. B1, *H. diversicolor* s.s. and *H. astae* sp. nov.) constitute an exception compared with the phylogeographic patterns observed in other European regions. Populations of *H. diversicolor* s.s. (Species A) and the remaining sympatric lineages (*Hediste* sp. B1 and *H. astae* sp. nov. (Species B4)) seem to split in the Skagerrak area, but alloenzyme data indicating sympatry between ‘Species A’ and ‘Species B’, or just the presence of Species B, were found in the Danish Ringkøbing fjord (Röhner *et al.*, 1997) and as well in the Weser Estuary (German North Sea coast; Fong & Garthwaite, 1994). Additional sampling in these areas could clarify if sympatry is indeed restricted only to the Skagerrak, Baltic and Kattegat Seas, or if it extends across the North Sea.

Cases of mismatch between alloenzymes and mitochondrial DNA in the Baltic Sea were interpreted by Audzijonyte *et al.* (2008) as indications of occasional hybridization some generations ago, that has led to mitochondrial introgression among Baltic lineages. This could justify the unusual intraspecific divergence patent in the ITS2 sequences of *Hediste* sp. B1, especially between the Mediterranean and Swedish populations. Our ITS2 data also show that Mediterranean haplotypes of *Hediste* sp. B1 displayed a high number of mutation steps, being clearly separated from the Swedish samples, whereas the Swedish haplotypes appear closer to *H. diversicolor* s.s. instead (Fig. 6). Furthermore, the presence of phylogenetically related haplotypes in the 28S locus between lineages from Norway and north of France (*H. diversicolor* s.s.) and the Swedish population (*Hediste* sp. B1), suggests that some level of gene flow may have occurred relatively recently. However, the occurrence of shared 28S haplotypes between different but closely related lineages (sorted by mitochondrial data) is not uncommon (e.g. Vieira *et al.*, 2019). This nuclear locus is known for its reliability in the reconstruction of deep phylogenies (e.g. Weitschek *et al.*, 2014), but can often fail to discriminate between species in many groups of animals (e.g. Jörger *et al.*, 2012).

Virgilio *et al.* (2009) hypothesized that Species A (*H. diversicolor* s.s.) colonized the Baltic from the North European Coasts after the Last Glacial Maximum. Given that the other sympatric lineages are missing from the NE Atlantic, they were probably introduced in the Baltic by human vectors through waterways from other European Seas (Black, Caspian or/and western

Mediterranean Sea). An example of this can be seen in the fish *Neogobius melanostomus* (Pallas, 1814), or the *Marenzelleria* Mesnil, 1896 polychaete species (Leppäkoski & Olenin, 2000; Sapota, 2004). This was also corroborated by both our and Audzijonyte *et al.*’s (2008) data, where the lack of genetic variability in the Baltic samples (Species B) and especially the low COI haplotype diversity in the Swedish population (MOTU 1, Table 3) suggests a recent bottleneck where the population would have been originated by a small number of colonizers, and did not have time for replenishing the variation through new mutations. Similar low diversity patterns were recorded for the European littoral prawn *Palaemon elegans* Rathke, 1836, where human vector-derived introductions into the Baltic from the Black Sea were also suggested (Reuschel *et al.*, 2010). Much of the present biological diversity of the Baltic is reported to be of foreign origin, composed of species intentionally or unintentionally moved by humans over intrinsic geographic barriers (Leppäkoski & Olenin, 2000).

As might have been expected, alloenzymes used in Audzijonyte *et al.* (2008) were not able to distinguish between *Hediste* sp. B1 and *H. astae* sp. nov., which corresponds to the species there referred to as ‘Species B’. The phylogenetic clades recovered in their study (BII and BIII corresponding to *H. astae* sp. nov. and BIV corresponding to *Hediste* sp. B1) did not indicate a subdivision into another pair of reproductively isolated biological lineages, since in the transition zone heterozygotes at the GOT-2 locus (alloenzyme) were commonly found. Indeed, our molecular data might not support complete reproductive isolation for the Swedish population (*Hediste* sp. B1), which also possesses low morphometric differentiation from *H. diversicolor* s.s. (Figs 22, 25–27). Additional ecological data are needed to reach more definitive conclusions, thereby this lineage remains unnamed in this study. On the other hand, *H. astae* sp. nov. (northern Aegean Sea) was both genetically and morphometrically very distinct, and no evidence of current hybridization was found in our study.

### New Mediterranean species

The Mediterranean Basin is a known biodiversity hotspot, in which taxa evolved and survived the Pleistocene cold phases, initiated circa 2.8 Ma (Hewitt, 1999, 2011; Maggs *et al.*, 2008; Myers *et al.*, 2000; Schmitt, 2007) and even reaching back to the Neogene, initiated circa 20.45 Ma (Husemann *et al.*, 2014). The presence of several closely related *Hediste* species in this region (*Hediste* sp. B1, *H. pontii* sp. nov., *Hediste* sp. B3 and *H. astae* sp. nov., Figs 3, 4) could be associated with the alternating glacial and interglacial stages. Assuming

that the *cytb* sequences from *Hediste* samples collected in Marseille (Breton et al., 2003) were not a result of anthropogenic transport, the Gibraltar Strait does not seem to be a contemporary prevention of gene flow between populations of *H. diversicolor* s.s. from the western Mediterranean and the north-east Atlantic. However, a geographic split separating *Hediste* sp. B1 from *H. diversicolor* s.s. appears to exist between the coast of Tuscany/Sardinia (Italy) and the Mediterranean coast of France. Additional samples from the Alboran Sea, Balearic Sea and South of France could be useful to check the occurrence of these lineages at a finer spatial scale.

The ancestral split of eastern Mediterranean lineages (*H. pontii* sp. nov., *Hediste* sp. B3 and *H. astae* sp. nov.) may be explained by the refugia in the Balkan Peninsula and Anatolia. There is a possibility that these refugia are not a single homogeneous unit but further sub-structured into a number of geographically small subunits, in which distinct lineages could have evolved while geographically separated (Gómez & Lunt, 2007; Schmitt et al., 2021), but further conclusions would require estimates of divergence times based on the genes (see Struck et al., 2018, Cerca et al., 2020), which is beyond the scope of this work. Furthermore, the low genetic diversity detected in the populations from the Adriatic Sea and the significant negative values found in the Tajima test for *H. pontii* sp. nov. (MOTU 3, Table 2) could be interpreted as an indication of a recent extinction and recolonization in this region. The particular topography and partially enclosed circulation of the Adriatic Sea (Artegiani et al., 1993) may have promoted the genetic isolation of these Adriatic populations. Similarly, the unique haplotypes observed in *Hediste* sp. B3 could be related to the isolation of the Amvrakikos Gulf and the periodic hypoxic conditions during its formation history (Vasileiadou et al., 2016). Moreover, there is the possibility that unsampled haplotypes occur in the area between Venice and Amvrakikos Lagoon, that hosts several potentially suitable habitats for this species. By comparing the pattern of *Hediste* to other brackish-water taxa, it could fit the one-direction stepping stone model, as observed in *Aphanius fasciatus* (Valenciennes, 1821); but with greater divergences due to shorter generation times and the very limited dispersal capability of any form of the life cycle (Langeneck et al., 2021). Thus, eastern Ionian Sea and northern Adriatic Sea haplotypes might well be two extremes of a continuum of unsampled populations.

The emergence of *H. astae* sp. nov., could be attributed to the different palaeoclimatic history of the Mediterranean and Black Seas. These two regions have specific environmental conditions (e.g. salinity, sea

surface temperature) which may have promoted the selection-driven divergence between the Mediterranean lineages (Peijnenburg et al., 2004, 2006). The colonization history of '*H. diversicolor*' in the Caspian Sea is probably recent since it is suspected that the species was introduced from the Black Sea in 1939–1941 (Grigorovich et al., 2003). Our samples from the northern Aegean Sea group in the same MOTU (Fig. 3) and have very low divergence compared with some sequences from the Caspian and Black Seas (Supplemental Fig. S1). It is possible that either *Hediste astae* sp. nov. has been transferred from the Baltic to the Black and Caspian Sea, or the opposite. We suspect it is primarily a Black Sea species that was secondarily introduced in the Baltic, because of (i) the parallel introduction in the Caspian Sea and (ii) the fact that this lineage appears closer to the eastern Mediterranean ones (*H. pontii* sp. nov. and *Hediste* sp. B3).

### **Intraspecific variation in *H. diversicolor* s.s**

*Hediste diversicolor* s.s. comprises a fair number of specimens (117) and sites sampled (9), extending from Portugal to Norway, where a clear genetic or geographic structure is hard to perceive (Figs 4, 5, Supplemental Fig. S3). Although within-clade COI genetic distances (up to 7.5%) are not as high as typical values found between congeneric polychaete species, they are much higher than what is usually observed within species, or even within species clades (<3%, Glasby, 2005; Paiva et al., 2019; Teixeira et al., 2022). High intraspecific COI variability was also observed in *H. astae* sp. nov., but to a far lesser extent (up to 3.5%). Mitochondrial genes have faster rates of nucleotide substitution compared with nuclear markers (Hebert et al., 2003a) and it is expected to find higher genetic distances in COI when compared with ITS2 or 28S loci. However, COI distances between *Hediste* lineages were also within the lower boundaries (max. divergence up to 10.1%) when compared with other polychaete studies (>15%, Carr et al., 2011; Lobo et al., 2016; Ravara et al., 2017; Sampieri et al., 2021), implying either a recent divergence or a case of an outlier species complex among polychaetes in what concerns patterns of COI variation. Interestingly, ITS2 intra- and interspecific distances were very similar to COI, and even had higher intra-specific values than this mitochondrial marker, including when separating the populations from Sweden and the western Mediterranean within MOTU 1 as well (Table 4). These findings deviate considerably from the typical pattern of low within-clade variation in DNA barcodes (COI) that has been reported for multiple animal taxa (Costa & Carvalho, 2010; Hebert et al., 2003b). The

fact that representative specimens of *H. diversicolor s.s.* from Portugal and Norway were ascribed respectively to as many as 26 and 7 different BINs, illustrates the uniqueness of this case. Seventy-seven haplotypes were recorded in 117 specimens, and, within the relatively small Lima estuary only, as many as 17 BINs have been attributed, 8 exclusive to this site (Table 3). The morphometric variation was also the highest among all the analysed lineages (17.51%, Table 6). Indeed, the unusually high level of variability in COI, and the absence of distinct ‘barcoding gaps’ (Hebert *et al.*, 2003b) within this highly variable lineage, contrasts with typical patterns of aggregation of COI barcodes in well-sorted clusters, which are commonly found, not only in polychaetes, but in marine invertebrates as well (Delić *et al.*, 2017; Desiderato *et al.*, 2019; Nygren *et al.*, 2018; Sá-Pinto *et al.*, 2008; Varela & Haye, 2012).

A range of possibilities could be proposed at this point to explain these observations, from mutation rates, through drift and selection. For example, Audzijonyte *et al.* (2008), reported high levels of mtDNA genetic diversity in some Baltic samples within Species A, and suggested that long-term isolation and subsequent mixing could have generated that pattern. However, the non-structured genealogy observed within the *H. diversicolor s.s.* clade is not suggestive of such history. Incipient speciation may also be an explanation. Svante Martinsson and Christer Erséus have discussed this phenomenon in cryptic Clitellata (Annelida) species, where a more restrictive approach to the species delimitation methods was taken. In particular, the species *Fridericia magna* Friend, 1899, failed to segregate using nuclear markers, despite having a large mitochondrial genetic variation (up to seven deep divergent lineages were retrieved). Hence the authors concluded it does not constitute a complex of cryptic species (Martinsson *et al.*, 2020), and suggested that each case should be seen as unique instead (Dupuis *et al.*, 2012; Martinsson & Erséus, 2021).

The genetic structure of *H. diversicolor* within estuaries could also be caused by a combination of stochastic biological and microevolutionary processes (i.e. short larval dispersal, sweepstake recruitment and genetic drift). Other alternative processes could be related to genetic adaptation of populations to environmental stressors. Toxicological studies showed that *H. diversicolor* can develop local ecotypes tolerant to high concentrations of heavy metals (Bryan & Hummerstone, 1971, 1973). The hypothesis of a genetic control of tolerance was supported by laboratory experiments demonstrating that tolerance to copper and zinc had a heritable component (Grant *et al.*, 1989). Patterns of differentiation in

alloenzymes, which could be related to the contamination levels, were found as well by Virgilio *et al.* (2003).

Currently available data for *H. diversicolor s.s.* are insufficient to attempt to provide any supported explanation for the patterns observed in this lineage. However, the exceptionality of this case merits detailed examination in future studies, which, due to its peculiarity, would require further and extensive sampling along the NE Atlantic to characterize as comprehensively as possible the genetic variability and the ecological features of this lineage.

## Conclusions

Formal description of cryptic species is particularly challenging since it depends largely on molecular data for which there is no established consensus on universal boundaries to delimit species (Lefébure *et al.*, 2006; Martinsson & Erséus, 2021; Moritz & Cicero, 2004; Westheide & Hass-Cordes, 2001). According to the phylogenetic species concept (Mishler & Theriot, 2000), and the mtDNA phylogroups definition (Avisé & Walker, 1999), reciprocal monophyly among mitochondrial clusters could be used as a criterion to consider all the five MOTUs of *H. diversicolor* as new species. However, according to the more restrictive biological species concept (Mayr, 1942), the molecular evidence obtained does not clearly support full reproductive isolation between two of the three sympatric lineages in the Baltic Sea (*Hediste* sp. B1 and *H. diversicolor s.s.*). Therefore, *Hediste* sp. B1 was not named in this study, requiring further reproductive and ecological data to clarify its taxonomic status. Similarly, low genetic distances between *H. pontii* sp. nov. and *Hediste* sp. B3, as well as lack of sufficient samples to test morphometric differentiation in the latter, also prevented reaching clear conclusions about that MOTU. Hence, the status of *Hediste* sp. B3 will remain uncertain until further samples can be examined, ideally through quantitative morphometric analysis, and additional data on reproductive and ecological features are available.

Describing and naming these species and similar cryptic complexes is essential, as understanding biodiversity is fundamental to ecological research and key to maintaining a healthy environment, understanding biogeographic patterns, or assessing and predicting climate change-induced impacts. Furthermore, considering the widespread use of *Hediste diversicolor* as a model organism or live bait, failing to recognize its true diversity may lead to undesired consequences. Different lineages can have different scope of environmental tolerance, making it difficult to compare between independent studies, and failure to appreciate the various

genetically or reproductively isolated lineages will probably affect the sustainability of their harvest.

## Acknowledgements

The authors would like to thank Massimo Ponti for the *Hediste* specimens from the Adriatic Sea; Eivind Oug for Norwegian specimens; Sarah Faulwetter for the large number of samples provided from several Greek locations in the northern Aegean Sea; Katerina Vasileidou for the northern Greek *Hediste* specimens; Julio Parapar for the Spanish samples; Juan Pardo for the northern French specimens; and lastly to Jorge Lobo and Claudia Hollatz for the help in collecting several *Hediste* samples in the Portuguese capital (Lisbon). Moreover, we would like to thank the reviewer and the Associate Editor Christoph Bleidorn for taking the time reviewing our manuscript.

SEM work was performed at the EMSO-PT Laboratory of Biodiversity and Connectivity & COBI, Universidade de Aveiro. EMSO-PT is funded by Portugal 2020, in the framework of COMPETE2020 (Programa Operacional Competitividade e Internacionalização-POCI), and FEDER (Fundo Europeu de Desenvolvimento Regional, ref. 01/SAICT/2016) and by national funds (OE), through FCT/MCTES (ref. PINFRA/22157/2016 EMSO-PT).

## Conflict of interests

The authors declare no conflicts of interest.

## Availability of data and materials

New sequence data and specimen metadata were uploaded in the project '*Hediste* species complex' (DS-MTHD) within BOLD (<http://v4.boldsystems.org/>) and in the following link: [dx.doi.org/10.5883/DS-MTHD](https://doi.org/10.5883/DS-MTHD). The alignments (FASTA and NEXUS formats) for each marker (COI, ITS2 and 28S) and the concatenated one (COI + ITS2 + 28S) are all publicly available online at Figshare (DOI: [dx.doi.org/10.6084/m9.figshare.19224600](https://doi.org/10.6084/m9.figshare.19224600)). GenBank accession numbers for the original data: OP038674-OP038788, OP038790-OP038834, OP038836-OP038897 (COI); OP028540-OP028635 (ITS2), and OP028725-OP028820 (28S). The new biological material is deposited at the Biological Research Collection (Marine Invertebrates) of the Department of Biology of the University of Aveiro (COBI at DBUA), Portugal, while specimens from Norway at the Norwegian University of Science and Technology, NTNU University Museum, all available upon request, with the exception of the ones exhausted in the DNA analysis mentioned in the Methods.

## Supplemental material

Supplemental material for this article can be accessed here: <https://doi.org/10.1080/14772000.2022.2116124>.

## Funding

This work was funded by the project 'River2Ocean – Socio-ecological and biotechnological solutions for the conservation and valorization of aquatic biodiversity in the Minho Region' (NORTE-01-0145-FEDER-000068), co-financed by the European Regional Development Fund (ERDF), through Programa Operacional Regional do Norte (NORTE 2020). Thanks are due, for the financial support to the Centre for Environmental and Marine Studies (CESAM, UIDB/50017/2020 + UIDP/50017/2020), to Portuguese Foundation for Science and Technology and Ministry of Education and Science (FCT/MEC) through national funds, and the co-funding by the FEDER, within the PT2020 Partnership Agreement and Compete 2020. The research leading to these results also received partial funding, from the European Union's Horizon 2020 research and innovation programme under grant agreement No 730984, ASSEMBLE Plus project (application no. 8229, 4th CALL, 'Crypticism in the marine realm: DNA barcode-based outlook into selected invertebrate taxa of the Eastern Mediterranean'). Marcos A.L. Teixeira was supported by a PhD grant from FCT (SFRH/BD/131527/2017), co-financed by the European Science Foundation (ESF). Pedro Vieira's work was supported by national funds through the Portuguese Foundation for Science and Technology (FCT, I.P.) in the scope of the project NIS-DNA (Early detection and monitoring of non-indigenous species in coastal ecosystems based on high-throughput sequencing tools, PTDC/BIA-BMA/29754/2017). Ascensão Ravara was funded by national funds, through FCT, I.P., in the scope of the framework contract foreseen in the numbers 4, 5 and 6 of article 23, of the Decree-Law 57/2016, of August 29, changed by Law 57/2017, of July 19. Financial support to Arne Nygren from the Norwegian Taxonomy Initiative [<http://www.biodiversity.no/Pages/135523>] (Cryptic polychaete species in Norwegian waters, knr 49-13, pnr 70184228), the Swedish Taxonomy Initiative [<https://www.artdatabanken.se/en/the-swedish-taxonomy-initiative/>] (Polychaete species complexes in Swedish waters, dnr 140/07 1.4 and 166/08 1.4), and Kungliga Fysiografiska sällskapet Nilsson-Ehle donationerna [<https://www.fysiografen.se/sv/>]. Financial support to Torkild Bakken from the Norwegian Taxonomy Initiative project Polychaetes in Norwegian Ports project no. 70184238.

## ORCID

Marcos A. L. Teixeira  <http://orcid.org/0000-0002-2228-2673>

Torkild Bakken  <http://orcid.org/0000-0002-5188-7305>

Pedro E. Vieira  <http://orcid.org/0000-0003-4880-3323>

Joachim Langeneck  <http://orcid.org/0000-0003-3665-8683>

Bruno R. Sampieri  <http://orcid.org/0000-0002-1675-1090>

Panagiotis Kasapidis  <http://orcid.org/0000-0002-1538-0320>

AscensãO Ravara  <http://orcid.org/0000-0002-1689-2985>

Arne Nygren  <http://orcid.org/0000-0001-5761-8803>

Filipe O. Costa  <http://orcid.org/0000-0001-5398-3942>

## References

- Anker, J. (1950). Otto Friderich Müller's Zoologia Danica. *Library Research Monograph*. 1 Munksgaard. 108.
- Artegiani, A., Gacic, M., Michelato, A., Kovacevic, V., Russo, A., Paschini, E., Scarazzato, P., & Smircic, A. (1993). The Adriatic Sea hydrography and circulation in spring and autumn (1985–1987). *Deep Sea Research Part II: Topical Studies in Oceanography*, 40, 1143–1180. [https://doi.org/10.1016/0967-0645\(93\)90065-U](https://doi.org/10.1016/0967-0645(93)90065-U)
- Astrin, J., Zhou, X., & Misof, B. (2013). The importance of biobanking in molecular taxonomy, with proposed definitions for vouchers in a molecular context. *ZooKeys*, 365, 67–70. <https://doi.org/10.3897/zookeys.365.5875>
- Audzijonyte, A., Ovcarenko, I., Bastrop, R., & Väinölä, R. (2008). Two cryptic species of the *Hediste diversicolor* group (Polychaeta, Nereididae) in the Baltic Sea, with mitochondrial signatures of different population histories. *Marine Biology*, 155, 599–612. <https://doi.org/10.1007/s00227-008-1055-3>
- Augener, H. (1933). Polychaeten aus den Zoologischen Museen von Leiden und Amsterdam. *Zoologische Mededeelingen s'Rijks Museum van Natuurlijke Historie Leiden*, 15, 177–260.
- Avise, J. C., & Walker, D. (1999). *Species realities and numbers in sexual vertebrates: Perspectives from an asexually transmitted genome* [Paper presentation]. Proceedings of the National Academy of Sciences, 96, 992–995.
- Bakken, T., Hårsaker, K., Daverdin, M. (2021). Marine invertebrate collection NTNU University Museum. Version 1.1269. Norwegian University of Science and Technology. Occurrence dataset <https://doi.org/10.15468/ddbs14> accessed via GBIF.org
- Bakken, T., Glasby, C. J., & Wilson, R. S. (2009). A review of paragnath morphology in Nereididae (Polychaeta). *Zoosymposia*, 2, 305–316. <https://doi.org/10.11646/zoosymposia.2.1.21>
- Bakken, T., & Wilson, R. S. (2005). Phylogeny of nereidids (Polychaeta, Nereididae) with paragnaths. *Zoologica Scripta*, 34, 507–547. <https://doi.org/10.1111/j.1463-6409.2005.00200.x>
- Bartels-Hardege, H. D., & Zeeck, E. (1990). Reproductive behaviour of *Nereis diversicolor* (Annelida: Polychaeta). *Marine Biology*, 106, 409–412. <https://doi.org/10.1007/BF01344320>
- Bouckaert, R., Heled, J., Kühnert, D., Vaughan, T., Wu, C. H., Xie, D., Suchard, M. A., Rambaut, A., & Drummond, A. J. (2014). BEAST 2: A Software Platform for Bayesian Evolutionary Analysis. *PLoS Computational Biology*, 10, e1003537. <https://doi.org/10.1371/journal.pcbi.1003537>
- Bowser, A. K., Diamond, A. W., & Addison, J. A. (2013). From Puffins to Plankton: A DNA-based analysis of a seabird food Chain in the Northern Gulf of Maine. *PLoS One*, 8, e83152. <https://doi.org/10.1371/journal.pone.0083152>
- Breton, S., Dufresne, F., Desrosiers, G., & Blier, P. U. (2003). Population structure of two northern hemisphere polychaetes, *Neanthes virens* and *Hediste diversicolor* (Nereididae), with different life-history traits. *Marine Biology*, 142, 707–715. <https://doi.org/10.1007/s00227-002-0992-5>
- Bryan, G. W., & Hummerstone, L. G. (1971). Adaptation of the polychaete *Nereis diversicolor* to estuarine sediments containing high concentrations of heavy metals. I. General observations and adaptation to copper. *Journal of the Marine Biological Association of the United Kingdom*, 51, 845–863. <https://doi.org/10.1017/S0025315400018014>
- Bryan, G. W., & Hummerstone, L. G. (1973). Adaptation of the polychaete *Hediste diversicolor* to estuarine sediments containing high concentrations of zinc and cadmium. *Journal of the Marine Biological Association of the United Kingdom*, 53, 839–857. <https://doi.org/10.1017/S0025315400022517>
- Burlinson, F. C., & Lawrence, A. J. (2007). A comparison of acute and chronic toxicity tests used to examine the temporal stability of a gradient in copper tolerance of *Hediste diversicolor* from the Fal estuary, Cornwall, UK. *Marine Pollution Bulletin*, 54, 66–71. <https://doi.org/10.1016/j.marpolbul.2006.08.047>
- Carr, C. M., Hardy, S. M., Brown, T. M., Macdonald, T. A., & Hebert, P. D. N. (2011). A Tri-Oceanic Perspective: DNA barcoding reveals geographic structure and cryptic diversity in Canadian polychaetes. *PLoS One*, 6, e22232. <https://doi.org/10.1371/journal.pone.0022232>
- Castresana, J. (2000). Selection of conserved blocks from multiple alignments for their use in phylogenetic analysis. *Molecular Biology and Evolution*, 17, 540–552. <https://doi.org/10.1093/oxfordjournals.molbev.a026334>
- Cerca, J., Meyer, C., Stateczny, D., Siemon, D., Wegbrod, J., Purschke, G., Dimitrov, D., & Struck, T. H. (2020). Deceleration of morphological evolution in a cryptic species complex and its link to paleontological stasis. *Evolution; International Journal of Organic Evolution*, 74, 116–131. <https://doi.org/10.1111/evo.13884>
- Chambers, S., & Garwood, P. (1992). *Polychaetes from Scottish Waters: A guide to identification 3. Family Nereididae*. National Museums of Scotland.
- Christensen, B. (1980). *Animal cytogenetics, vol 2, Annelida*. Gebrüder Borntraeger.
- Clarke, K. R., & Warwick, R. M. (2001). A further biodiversity index applicable to species lists: variation in taxonomic distinctness. *Marine Ecology Progress Series*, 216, 265–278. <https://doi.org/10.3354/meps216265>

- Clement, M., Snell, Q., Walke, P., Posada, D., & Crandall, K. (2002). *TCS: estimating gene genealogies* [Paper presentation]. Proceedings 16th International Parallel and Distributed Processing Symposium, 7 pp.
- Conde-Vela, V. M., & Salazar-Vallejo S. I. (2015). Redescriptions of *Nereis oligohalina* (Rioja, 1946) and *N. garwoodi* González-Escalante & Salazar-Vallejo, 2003 and description of *N. confusa* sp. n. (Annelida, Nereididae). *ZooKeys*, 518, 15–49.
- Costa, F. O., & Carvalho, G. R. (2010). New insights into molecular evolution: prospects from the Barcode of Life Initiative (BOL). *Theory in Biosciences = Theorie in Den Biowissenschaften*, 129, 149–157.
- Cuny, P., Miralles, G., Cornet-Barthaux, V., Acquaviva, M., Stora, G., Grossi, V., & Gilbert, F. (2007). Influence of bioturbation by the polychaete *Nereis diversicolor* on the structure of bacterial communities in oil contaminated coastal sediments. *Marine Pollution Bulletin*, 54, 452–459. <https://doi.org/10.1016/j.marpolbul.2006.12.008>
- Dales, R. P. (1950). The reproduction and larval development of *Nereis diversicolor* O. F. Müller. *Journal of the Marine Biological Association of the United Kingdom*, 29, 321–360. <https://doi.org/10.1017/S0025315400055405>
- Darriba, D., Taboada, G. L., Doallo, R., & Posada, D. (2012). jModelTest 2: more models, new heuristics and parallel computing. *Nature Methods*, 9, 772–772. <https://doi.org/10.1038/nmeth.2109>
- Delić, T., Trontelj, P., Rendoš, M., & Fišer, C. (2017). The importance of naming cryptic species and the conservation of endemic subterranean amphipods. *Scientific Reports*, 7, 3391. <https://doi.org/10.1038/s41598-017-02938-z>
- Desiderato, A., Costa, F. O., Serejo, C. S., Abbiati, M., Queiroga, H., & Vieira, P. E. (2019). Macaronesian islands as promoters of diversification in amphipods: The remarkable case of the family Hyalidae (Crustacea, Amphipoda). *Zoologica Scripta*, 48, 359–375. <https://doi.org/10.1111/zsc.12339>
- Dupuis, J. R., Roe, A. D., & Sperling, F. A. H. (2012). Multi-locus species delimitation in closely related animals and fungi: one marker is not enough. *Molecular Ecology*, 21, 4422–4436. <https://doi.org/10.1111/j.1365-294X.2012.05642.x>
- Durou, C., Mouneyrac, C., & Amiard-Triquet, C. (2005). Tolerance to metals and assessment of energy reserves in the polychaete *Nereis diversicolor* in clean and contaminated estuaries. *Environmental Toxicology*, 20, 23–31. <https://doi.org/10.1002/tox.20074>
- Durou, C., Smith, B. D., Roméo, M., Rainbow, P. S., Mouneyrac, C., Mouloud, M., Gnassia-Barelli, M., Gillet, P., Deutch, B., & Amiard-Triquet, C. (2007). From biomarkers to population responses in *Nereis diversicolor*: Assessment of stress in estuarine ecosystems. *Ecotoxicology and Environmental Safety*, 66, 402–411. <https://doi.org/10.1016/j.ecoenv.2006.02.016>
- Einfeldt, A. L., Doucet, J. R., & Addison, J. A. (2014). Phylogeography and cryptic introduction of the ragworm *Hediste diversicolor* (Annelida, Nereididae) in the Northwest Atlantic. *Invertebrate Biology*, 133, 232–241. <https://doi.org/10.1111/ivb.12060>
- Faulwetter, S., Markantonatou, V., Pavlouidi, C., Papageorgiou, N., Keklikoglou, K., Chatzinikolaou, E., Pafilis, E., Chatzigeorgiou, G., Vasileiadou, K., Dailianis, T., Fanini, L., Koulouri, P., & Arvanitidis, C. (2014). Polytraits: A database on biological traits of marine polychaetes. *Biodiversity Data Journal*, 2, e1024. <https://doi.org/10.3897/BDJ.2.e1024>
- Fauvel, P. (1923). Polychètes errantes. *Faune de France*, 5, 1–488.
- Fišer, C., Robinson, C. T., & Malard, F. (2018). Cryptic species as a window into the paradigm shift of the species concept. *Molecular Ecology*, 27, 613–635. <https://doi.org/10.1111/mec.14486>
- Fong, P. P., & Garthwaite, R. L. (1994). Allozyme electrophoretic analysis of the *Hediste limnicola* – *H. diversicolor* – *H. japonica* species complex (Polychaeta: Nereididae). *Marine Biology*, 118, 463–470. <https://doi.org/10.1007/BF00350303>
- Forsman, A. (2015). Rethinking phenotypic plasticity and its consequences for individuals, populations and species. *Heredity*, 115, 276–284. <https://doi.org/10.1038/hdy.2014.92>
- Friend, H. (1899). New British annelids. *The Zoologist (Series 4)* 3, 262–265.
- Fujisawa, T., & Barraclough, T. G. (2013). Delimiting species using single-locus data and the Generalized Mixed Yule Coalescent Approach: A revised method and evaluation on simulated data sets. *Systematic Biology*, 62, 707–724. <https://doi.org/10.1093/sysbio/syt033>
- Fusco, G., & Minelli, A. (2010). Phenotypic plasticity in development and evolution: facts and concepts. *Philosophical Transactions of the Royal Society B: Biological Sciences*, 365, 547–556. <https://doi.org/10.1098/rstb.2009.0267>
- Galil, B. S., Clark, P. F., & Carlton, J. T. (2011). *In the Wrong Place—Alien Marine Crustacean: Distribution, Biology, and Impacts*. Springer.
- Glasby, C. J. (2005). Polychaete Distribution Patterns Revisited: an historical explanation. *Marine Ecology*, 26, 235–245. <https://doi.org/10.1111/j.1439-0485.2005.00059.x>
- Gomes-dos-Santos, A., Hagemann, A., Valente, L., Malzahn, A. M., Monroig, Ó., Froufe, E., & Castro, L. F. C. (2021). Complete mitochondrial genome of the ragworm annelid *Hediste diversicolor* (of Müller, 1776) (Annelida: Nereididae). *Mitochondrial DNA. Part B, Resources*, 6, 2849–2851. <https://doi.org/10.1080/23802359.2021.1970644>
- Gómez, A., & Lunt, D. H. (2007). Refugia within Refugia: Patterns of phylogeographic concordance in the Iberian Peninsula. In S. Weiss & N. Ferrand (Eds.), *Phylogeography of Southern European Refugia* (pp. 155–188). Springer.
- Gorley, C. K., & Clarke, K. (2006) *PRIMER v6: user manual/tutorial*. PRIMER-E, Plymouth, UK.
- Grant, A., Hateley, J. G., & Jones, N. V. (1989). Mapping the ecological impact of heavy metals on the estuarine polychaete *Nereis diversicolor* using inherited metal tolerance. *Marine Pollution Bulletin*, 20, 235–238. [https://doi.org/10.1016/0025-326X\(89\)90438-4](https://doi.org/10.1016/0025-326X(89)90438-4)
- Grigorovich, I. A., Therriault, T. W., & MacIsaac, H. J. (2003). History of aquatic invertebrate invasions in the Caspian Sea. *Biological Invasions*, 5, 103–115. <https://doi.org/10.1023/A:1024050824073>
- Guindon, S., & Gascuel, O. (2003). A Simple, Fast, and Accurate Algorithm to Estimate Large Phylogenies by Maximum Likelihood. *Systematic Biology*, 52, 696–704. <https://doi.org/10.1080/10635150390235520>
- Hartmann-Schröder, G. (1996). *Annelida, Borstenwürmer, Polychaeta*. Gustav Fischer.
- Hateley, J. G., Grant, A., Taylor, S. M., & Jones, N. V. (1992). Morphological and other evidence on the degree of

- genetic differentiation between populations of *Nereis diversicolor*. *Journal of the Marine Biological Association of the United Kingdom*, 72, 365–381. <https://doi.org/10.1017/S0025315400037760>
- Hebert, P. D. N., Cywinska, A., Ball, S. L., & deWaard, J. R. (2003a) *Biological identifications through DNA barcodes* [Paper presentation]. Proceedings of the Royal Society of London. Series B: Biological Sciences, 270, 313–321. <https://doi.org/10.1098/rspb.2002.2218>
- Hebert, P. D. N., Ratnasingham, S., & de Waard, J. R. (2003b). Barcoding animal life: cytochrome c oxidase subunit 1 divergences among closely related species. *Proceedings of the Royal Society of London. Series B: Biological Sciences*, 270, S96–S99. <https://doi.org/10.1098/rsbl.2003.0025>
- Hewitt, G. M. (1999). Post-glacial re-colonization of European biota. *Biological Journal of the Linnean Society*, 68, 87–112. <https://doi.org/10.1111/j.1095-8312.1999.tb01160.x>
- Hewitt, G. M. (2011). Mediterranean peninsulas: the evolution of hotspots. In F. E. Zachos & J. C. Habel (Eds.), *Biodiversity Hotspots: Distribution and protection of conservation priority areas* (pp. 123–147). Springer.
- Husemann, M., Schmitt, T., Zachos, F. E., Ulrich, W., & Habel, J. C. (2014). Palaeoarctic biogeography revisited: evidence for the existence of a North African refugium for Western Palaeoarctic biota. *Journal of Biogeography*, 41, 81–94. <https://doi.org/10.1111/jbi.12180>
- Hutchings, P., & Kupriyanova, E. (2018). Cosmopolitan polychaetes – fact or fiction? Personal and historical perspectives. *Invertebrate Systematics*, 32, 1–9. <https://doi.org/10.1071/IS17035>
- Izuka, A. (1908). On the breeding habit and development of *Nereis japonica* n. sp. *Annotationes Zoologicae Japonenses*, 6, 295–305.
- Jörger, K. M., Norenburg, J. L., Wilson, N. G., & Schrödl, M. (2012). Barcoding against a paradox? Combined molecular species delineations reveal multiple cryptic lineages in elusive meiofaunal sea slugs. *BMC Evolutionary Biology*, 12, 245. <https://doi.org/10.1186/1471-2148-12-245>
- Katoh, K., & Standley, D. M. (2013). MAFFT Multiple Sequence Alignment Software Version 7: Improvements in Performance and Usability. *Molecular Biology and Evolution*, 30, 772–780. <https://doi.org/10.1093/molbev/mst010>
- Kristensen, E. (1983). Ventilation and oxygen uptake by three species of *Nereis* (Annelida: Polychaeta). I. Effects of hypoxia. *Marine Ecology Progress Series*, 12, 289–297. <https://doi.org/10.3354/meps012289>
- Kumar, S., Stecher, G., Li, M., Knyaz, C., & Tamura, K. (2018). MEGA X: Molecular Evolutionary Genetics Analysis across computing platforms. *Molecular Biology and Evolution*, 35, 1547–1549. <https://doi.org/10.1093/molbev/msy096>
- Langeneck, J., Englezou, C., Di Maggio, M., Castelli, A., & Maltagliati, F. (2021). Phylogeography of *Aphanius fasciatus* (Osteichthyes: Aphaniidae) in the Mediterranean Sea, with a focus on its conservation in Cyprus. *Hydrobiologia*, 848, 4093–4114. <https://doi.org/10.1007/s10750-021-04627-5>
- Lefébure, T., Douady, C. J., Gouy, M., & Gibert, J. (2006). Relationship between morphological taxonomy and molecular divergence within Crustacea: Proposal of a molecular threshold to help species delimitation. *Molecular Phylogenetics and Evolution*, 40, 435–447. <https://doi.org/10.1016/j.ympev.2006.03.014>
- Leigh, J. W., & Bryant, D. (2015). Popart: full-feature software for haplotype network construction. *Methods in Ecology and Evolution*, 6, 1110–1116. <https://doi.org/10.1111/2041-210X.12410>
- Leppäkoski, E., & Olenin, S. (2000). Non-native Species and Rates of Spread: Lessons from the Brackish Baltic Sea. *Biological Invasions*, 2, 151–163. <https://doi.org/10.1023/A:1010052809567>
- Librado, P., & Rozas, J. (2009). DnaSP v5: a software for comprehensive analysis of DNA polymorphism data. *Bioinformatics (Oxford, England)*, 25, 1451–1452.
- Lobo, J., Teixeira, M. A. L., Borges, L. M. S., Ferreira, M. S. G., Hollatz, C., Gomes, P. T., Sousa, R., Ravara, A., Costa, M. H., & Costa, F. O. (2016). Starting a DNA barcode reference library for shallow water polychaetes from the southern European Atlantic coast. *Molecular Ecology Resources*, 16, 298–313. <https://doi.org/10.1111/1755-0998.12441>
- Mags, C. A., Castilho, R., Foltz, D., Henzler, C., Jolly, M. T., Kelly, J., Olsen, J., Perez, K. E., Stam, W., Väinölä, R., Viard, F., & Wares, J. (2008). Evaluating Signatures of Glacial Refugia for North Atlantic Benthic Marine Taxa. *Ecology*, 89, S108–S122. <https://doi.org/10.1890/08-0257.1>
- Maltagliati, F., Massaro, L., Cossu, P., & Castelli, A. (2006). Morphological differentiation in the ragworm, *Hediste diversicolor* (Polychaeta, Nereididae), as revealed by variation of paragnath number and distribution. *Italian Journal of Zoology*, 73, 255–262. <https://doi.org/10.1080/11250000600700052>
- Malmgren, A. J. (1867). *Annulata Polychaeta Spetsbergiae, Groenlandiae, Islandiae et Scandinaviae hactenus cognita*. Frenckelliana, Helsingforsiae [Helsinki].
- Martin, D., Meca, M. A., Gil, J., Drake, P., & Nygren, A. (2017). Another brick in the wall: population dynamics of a symbiotic species of *Oxydromus* (Annelida, Hesioniidae), described as new based on morphometry. *Contributions to Zoology*, 86, 181–211. <https://doi.org/10.1163/18759866-08603001>
- Martinsson, S., & Erséus, C. (2021). Cryptic Clitellata: Molecular Species Delimitation of Clitellate Worms (Annelida): An Overview. *Diversity*, 13, 36. <https://doi.org/10.3390/d13020036>
- Martinsson, S., Klinth, M., & Erséus, C. (2020). Testing species hypotheses for *Fridericia magna*, an enchytraeid worm (Annelida: Clitellata) with great mitochondrial variation. *BMC Evolutionary Biology*, 20, 116. <https://doi.org/10.1186/s12862-020-01678-5>
- Mayr, E. (1942). *Systematics and the Origin of Species*. Columbia University Press.
- Mesnil, F. (1896). Études de morphologie externe chez les Annélides. I. Les Spionidiens des côtes de la Manche. *Bulletin Scientifique de la France et de la Belgique*. 29, 110–287, plates VII–XV. <https://doi.org/10.5962/bhl.part.19052>
- Mishler, B. D., & Theriot, E. (2000). The phylogenetic species concept sensu Mishler and Theriot: monophyly, apomorphy, and phylogenetic species concepts. In Q. D. Wheeler & E. Meier (Eds), *Species Concepts and Phylogenetic Theory: A Debate* (pp. 44–54). Columbia University Press.
- Moreira, S. M., Lima, I., Ribeiro, R., & Guilhermino, L. (2006). Effects of estuarine sediment contamination on feeding and on key physiological functions of the

- polychaete *Hediste diversicolor*: Laboratory and in situ assays. *Aquatic Toxicology (Amsterdam, Netherlands)*, 78, 186–201. <https://doi.org/10.1016/j.aquatox.2006.03.001>
- Moritz, C., & Cicero, C. (2004). DNA Barcoding: Promise and Pitfalls. *PLoS Biology*, 2, e354. <https://doi.org/10.1371/journal.pbio.0020354>
- Müller, O. F. (1776). *Zoologiae Danicae prodromus: seu Animalium Daniae et Norvegiae indigenarum; characteres, nomina, et synonyma imprimis popularium* (pp. 282). Hallageriis: Havniae (Copenhagen).
- Myers, N., Mittermeier, R. A., Mittermeier, C. G., da Fonseca, G. A. B., & Kent, J. (2000). Biodiversity hotspots for conservation priorities. *Nature*, 403, 853–858. <https://doi.org/10.1038/35002501>
- Neuhoff, H. G. (1979). Influence of temperature and salinity on food conversion and growth of different *Nereis* species (Polychaeta Annelida). *Marine Ecology Progress Series*, 1, 255–262. <https://doi.org/10.3354/meps001255>
- Nygren, A., Parapar, J., Pons, J., Meißner, K., Bakken, T., Kongsrud, J. A., Oug, E., Gaeva, D., Sikorski, A., Johansen, R. A., Hutchings, P. A., Lavesque, N., & Capa, M. (2018). A mega-cryptic species complex hidden among one of the most common annelids in the North East Atlantic. *PLoS One*, 13, e0198356. <https://doi.org/10.1371/journal.pone.0198356>
- Oug, E., Bakken, T., & Kongsrud, J. A. (2014). Original specimens and type localities of early described polychaete species (Annelida) from Norway, with particular attention to species described by O.F. Müller and M. Sars. *Memoirs of Museum Victoria*, 71, 217–236. <https://doi.org/10.24199/j.mmv.2014.71.17>
- Paiva, P. C., Mutaquilha, B. F., Coutinho, M. C. L., & Santos, C. S. G. (2019). Comparative phylogeography of two coastal species of *Perinereis* Kinberg, 1865 (Annelida, Polychaeta) in the South Atlantic. *Marine Biodiversity*, 49, 1537–1551. <https://doi.org/10.1007/s12526-018-0927-0>
- Patarnello, T., Volckaert, F. A. M. J., & Castilho, R. (2007). Pillars of Hercules: is the Atlantic–Mediterranean transition a phylogeographical break? *Molecular Ecology*, 16, 4426–4444. <https://doi.org/10.1111/j.1365-294X.2007.03477.x>
- Peijnenburg, K. T. C. A., Breeuwer, J. A. J., Pierrot-Bults, A. C., & Menken, S. B. J. (2004). Phylogeography of the Planktonic Chaetognath *Sagitta Setosa* Reveals Isolation in European Seas. *Evolution; International Journal of Organic Evolution*, 58, 1472–1487. <https://doi.org/10.1111/j.0014-3820.2004.tb01728.x>
- Peijnenburg, K. T. C. A., Fauvelot, C., Breeuwer, J. A. J., & Menken, S. B. J. (2006). Spatial and temporal genetic structure of the planktonic *Sagitta setosa* (Chaetognatha) in European seas as revealed by mitochondrial and nuclear DNA markers. *Molecular Ecology*, 15, 3319–3338. <https://doi.org/10.1111/j.1365-294X.2006.03002.x>
- Pleasant Bay Community Boating (PBCB) Bioblitz 2016 by Ocean Genome Legacy. Sequences available at BOLD. [http://v4.boldsystems.org/index.php/Public\\_BarcodeCluster?clusteruri=BOLD:AD11892](http://v4.boldsystems.org/index.php/Public_BarcodeCluster?clusteruri=BOLD:AD11892)
- Pleijel, F., Jondelius, U., Norlinder, E., Nygren, A., Oxelman, B., Schander, C., Sundberg, P., & Thollessen, M. (2008). Phylogenies without roots? A plea for the use of vouchers in molecular phylogenetic studies. *Molecular Phylogenetics and Evolution*, 48, 369–371 <https://doi.org/10.1016/j.ympev.2008.03.024>
- Puillandre, N., Lambert, A., Brouillet, S., & Achaz, G. (2012). ABGD, Automatic Barcode Gap Discovery for primary species delimitation. *Molecular Ecology*, 21, 1864–1877. <https://doi.org/10.1111/j.1365-294X.2011.05239.x>
- R Core Team. (2019). *R: A language and environment for statistical computing*. R Foundation for Statistical Computing. <https://www.R-project.org/>
- Rambaut, A., Drummond, A. J., Xie, D., Baele, G., & Suchard, M. A. (2018). Posterior Summarization in Bayesian Phylogenetics Using Tracer 1.7. *Systematic Biology*, 67, 901–904. <https://doi.org/10.1093/sysbio/syy032>
- Rathke, H. (1836). Zur Fauna der Krym. *Mémoires de l'Académie Impériale des Sciences de Saint Pétersbourg*, 3, 291–454.
- Ratnasingham, S., & Hebert, P. D. N. (2013). A DNA-Based Registry for All Animal Species: The Barcode Index Number (BIN) System. *PLoS One*, 8, e66213. <https://doi.org/10.1371/journal.pone.0066213>
- Ravara, A., Ramos, D., Teixeira, M. A. L., Costa, F. O., & Cunha, M. R. (2017). Taxonomy, distribution and ecology of the order Phyllodocida (Annelida, Polychaeta) in deep-sea habitats around the Iberian margin. *Deep Sea Research Part II: Topical Studies in Oceanography*, 137, 207–231. <https://doi.org/10.1016/j.dsr2.2016.08.008>
- Reuschel, S., Cuesta, J. A., & Schubart, C. D. (2010). Marine biogeographic boundaries and human introduction along the European coast revealed by phylogeography of the prawn *Palaeomon elegans*. *Molecular Phylogenetics and Evolution*, 55, 765–775. <https://doi.org/10.1016/j.ympev.2010.03.021>
- Röhner, M., Bastrop, R., & Jürss, K. (1997). Genetic differentiation in *Hediste diversicolor* (Polychaeta: Nereididae) for the North Sea and the Baltic Sea. *Marine Biology*, 130, 171–180. <https://doi.org/10.1007/s002270050236>
- Ronquist, F., & Huelsenbeck, J. P. (2003). MrBayes 3: Bayesian phylogenetic inference under mixed models. *Bioinformatics*, 19, 1572–1574. [Database] <https://doi.org/10.1093/bioinformatics/btg180>
- Salazar-Vallejo, S. I., de León-Gonzalez, J. A., & Conde-Vela, V. M. (2021). Revision of the species confused with “*Nereis falsa*” de Quatrefages, 1866 (Annelida, Nereididae). *European Journal of Taxonomy*, 779, 1–70. <https://doi.org/10.5852/ejt.2021.779.1579>
- Sampieri, B. R., Vieira, P. E., Teixeira, M. A. L., Seixas, V. C., Pagliosa, P. R., Amaral, A. C. Z., & Costa, F. O. (2021). Molecular diversity within the genus *Laeonereis* (Annelida, Nereididae) along the west Atlantic coast: paving the way for integrative taxonomy. *PeerJ*, 9, e11364. <https://doi.org/10.7717/peerj.11364>
- Sá-Pinto, A., Branco, M., Sayanda, D., & Alexandrino, P. (2008). Patterns of colonization, evolution and gene flow in species of the genus *Patella* in the Macaronesian Islands. *Molecular Ecology*, 17, 519–532. <https://doi.org/10.1111/j.1365-294X.2007.03563.x>
- Sapota, M. R. (2004). The round goby (*Neogobius melanostomus*) in the Gulf of Gdańsk — a species introduction into the Baltic Sea. In H. Kautsky & P. Snoeijis (Eds.), *Developments in Hydrobiology* (pp. 219–224). *Biology of the Baltic Sea* Springer Netherlands.
- Sars, M. (1835). *Beskrivelser og Iagttagelser over nogle moerkelige eller nye i Havet ved den Bergenske Kyst levende Dyr af Polypernes, Acalepernes, Radiaternes, Annelidernes og Molluskernes classer, med en kort Oversigt over de hidtil af Forfatteren sammesteds fundne Arter og*

- deres Forekommen* (xii + 81 pp., 15 plates). Thorstein Hallagers Forlag hos Chr. Dahl, R.S.
- Sato, M., & Nakashima, A. (2003). A review of Asian *Hediste* species complex (Nereididae, Polychaeta) with descriptions of two new species and a redescription of *Hediste japonica* (Izuka, 1908). *Zoological Journal of the Linnean Society*, 137, 403–445. <https://doi.org/10.1046/j.1096-3642.2003.00059.x>
- Scaps, P. (2002). A review of the biology, ecology and potential use of the common ragworm *Hediste diversicolor* (O.F. Müller) (Annelida: Polychaeta). *Hydrobiologia*, 470, 203–218. <https://doi.org/10.1023/A:1015681605656>
- Schmitt, T. (2007). Molecular biogeography of Europe: Pleistocene cycles and postglacial trends. *Frontiers in Zoology*, 4, 11. <https://doi.org/10.1186/1742-9994-4-11>
- Schmitt, T., Fritz, U., Delfino, M., Ulrich, W., & Habel, J. C. (2021). Biogeography of Italy revisited: genetic lineages confirm major phylogeographic patterns and a pre-Pleistocene origin of its biota. *Frontiers in Zoology*, 18, 34. <https://doi.org/10.1186/s12983-021-00418-9>
- Smith, R. I. (1950). Embryonic development in the viviparous nereid polychaete, *Neanthes lighti* hartman. *Journal of Morphology*, 87, 417–465. <https://doi.org/10.1002/jmor.1050870303>
- Smith, R. I. (1964). On the early development of *Nereis diversicolor* in different salinities. *Journal of Morphology*, 114, 437–463. <https://doi.org/10.1002/jmor.1051140306>
- Ström, H. (1762). *Physisk og Oeconomisk Beskrivelse over Fogderiet Søndmør, beliggende i Bergens Stift i Norge! Saelges i Rothes Enkes og Profits Boghandling*. Kiøbenhavn. 1143
- Struck, T. H., Feder, J. L., Bendiksby, M., Birkeland, S., Cerca, J., Gusarov, V. I., Kistenich, S., Larsson, K. H., Liow, L. H., Nowak, M. D., Stedje, B., Bachmann, L., & Dimitrov, D. (2018). Finding Evolutionary Processes Hidden in Cryptic Species. *Trends in Ecology & Evolution*, 33, 153–163. <https://doi.org/10.1016/j.tree.2017.11.007>
- Teixeira, M. A. L., Vieira, P. E., Pleijel, F., Sampieri, B. R., Ravara, A., Costa, F. O., & Nygren, A. (2020). Molecular and morphometric analyses identify new lineages within a large *Eumida* (Annelida) species complex. *Zoologica Scripta*, 49, 222–235. <https://doi.org/10.1111/zsc.12397>
- Teixeira, M. A. L., Vieira, P. E., Ravara, A., Costa, F. O., & Nygren, A. (2022). From 13 to 22 in a second stroke: revisiting the European *Eumida sanguinea* (Phyllococidae: Annelida) species complex. *Zoological Journal of the Linnean Society*, 196, 169–197. <https://doi.org/10.1093/zoolinnean/zlab100>
- Tosuji, H., Bastrop, R., Götting, M., Park, T., Hong, J. S., & Sato, M. (2019). Worldwide molecular phylogeny of common estuarine polychaetes of the genus *Hediste* (Annelida: Nereididae), with special reference to interspecific common haplotypes found in southern Japan. *Marine Biodiversity*, 49, 1385–1402. <https://doi.org/10.1007/s12526-018-0917-2>
- Varela, I. A., & Haye, P. A. (2012). The marine brooder *Excirrolana braziliensis* (Crustacea: Isopoda) is also a complex of cryptic species on the coast of Chile. *Revista Chilena de Historia Natural*, 85, 495–502. <https://doi.org/10.4067/S0716-078X2012000400011>
- Vasileiadou, K., Pavloudi, C., Sarpoulou, E., Fragopoulou, N., Kotoulas, G., & Arvanitidas, C. (2016). Unique COI haplotypes in *Hediste diversicolor* populations in lagoons adjoining the Ionian Sea. *Aquatic Biology*, 25, 7–15. <https://doi.org/10.3354/ab00654>
- Vieira, P. E., Desiderato, A., Holdich, D. M., Soares, P., Creer, S., Carvalho, G. R., Costa, F. O., & Queiroga, H. (2019). Deep segregation in the open ocean: Macaronesia as an evolutionary hotspot for low dispersal marine invertebrates. *Molecular Ecology*, 28, 1784–1800. <https://doi.org/10.1111/mec.15052>
- Villalobos-Guerrero, T. F., & Carrera-Parra, L. F. (2015). Redescription of *Alitta succinea* (Leuckart, 1847) and reinstatement of *A. acutifolia* (Ehlers, 1901) n. comb. based upon morphological and molecular data (Polychaeta: Nereididae). *Zootaxa*, 3919, 157–178. <https://doi.org/10.11646/zootaxa.3919.1.7>
- Villalobos-Guerrero, T. F. (2019). Redescription of two overlooked species of the *Perinereis nuntia* complex and morphological delimitation of *P. nuntia* (Savigny in Lamarck, 1818) from the Red Sea (Annelida, Nereididae). *Zoosystema*, 41, 465–496. <https://doi.org/10.5252/zoosystema2019v41a24>
- Villalobos-Guerrero, T. F., & Bakken, T. (2018). Revision of the *Alitta virens* species complex (Annelida: Nereididae) from the North Pacific Ocean. *Zootaxa*, 4483, 201–257.
- Virgilio, M., & Abbiati, M. (2006). Temporal changes in the genetic structure of intertidal populations of *Hediste diversicolor* (Polychaeta: Nereididae). *Journal of Sea Research*, 56, 53–58. <https://doi.org/10.1016/j.seares.2006.03.008>
- Virgilio, M., Baroncini, N., Trombini, C., & Abbiati, M. (2003). Relationships between sediments and tissue contamination and allozymic patterns in *Hediste diversicolor* (Polychaeta Nereididae) in the Pialassa lagoons (north Adriatic Sea). *Oceanologica Acta*, 26, 85–92 [https://doi.org/10.1016/S0399-1784\(02\)01230-6](https://doi.org/10.1016/S0399-1784(02)01230-6)
- Virgilio, M., Fauvelot, C., Costantini, F., Abbiati, M., & Backeljau, T. (2009). Phylogeography of the common ragworm *Hediste diversicolor* (Polychaeta: Nereididae) reveals cryptic diversity and multiple colonization events across its distribution. *Molecular Ecology*, 18, 1980–1994. <https://doi.org/10.1111/j.1365-294X.2009.04170.x>
- Virgilio, M., Maci, S., & Abbiati, M. (2005). Comparisons of genotype-tolerance responses in populations of *Hediste diversicolor* (Polychaeta: Nereididae) exposed to copper stress. *Marine Biology*, 147, 1305–1312. <https://doi.org/10.1007/s00227-005-0030-5>
- Volkenborn, N., Hedtkamp, S. I. C., van Beusekom, J. E. E., & Reise, K. (2007). Effects of bioturbation and bioirrigation by lugworms (*Arenicola marina*) on physical and chemical sediment properties and implications for intertidal habitat succession. *Estuarine, Coastal and Shelf Science*, 74, 331–343. <https://doi.org/10.1016/j.ecss.2007.05.001>
- Wares, J. P., & Cunningham, C. W. (2001). Phylogeography and historical ecology of the North Atlantic Intertidal. *Evolution; International Journal of Organic Evolution*, 55, 2455–2469.
- Weitschek, E., Fison, G., & Felici, G. (2014). Supervised DNA Barcodes species classification: analysis, comparisons and results. *BioData Mining*, 7, 4. <https://doi.org/10.1186/1756-0381-7-4>
- Westheide & Hass-Cordes. (2001). Molecular taxonomy: description of a cryptic *Petitia* species (Polychaeta: Syllidae) from the island of Mahé (Seychelles, Indian Ocean) using RAPD markers and ITS2 sequences. *Journal of Zoological Systematics and Evolutionary Research*, 39, 103–111. <https://doi.org/10.1046/j.1439-0469.2001.00166.x>

- Wolff, W. J. (1973). The estuary as a habitat an analysis of data on the soft-bottom Macrofauna of the Estuarine area of the rivers rhine, Meuse, and Scheldt. *Zoologische Verhandelingen*, 126, 1–242.
- Xavier, J. R., & Van Soest, R. W. M. (2012). Diversity patterns and zoogeography of the Northeast Atlantic and Mediterranean shallow-water sponge fauna. *Hydrobiologia*, 687, 107–125. <https://doi.org/10.1007/s10750-011-0880-4>
- Younsi, M., Daas, T., Daas, O., & Scaps, P. (2010). Polychaetes of commercial interest from the Mediterranean East Coast of Algeria. *Mediterranean Marine Science*, 11, 185–188. <https://doi.org/10.12681/mms.101>
- Zhang, J., Kapli, P., Pavlidis, P., & Stamatakis, A. (2013). A general species delimitation method with applications to phylogenetic placements. *Bioinformatics (Oxford, England)*, 29, 2869–2876. <https://doi.org/10.1093/bioinformatics/btt499>

**Associate Editor: Dr Christoph Bleidorn**